Invited Review

Advanced metallization schemes for bonding of InP-based laser devices to CVD-diamond heatsinks

A. Katz, C.H. Lee and K.L. Tai
AT&T Bell Laboratories, Murray Hill, NJ 07974 (USA)

(Received June 17, 1993)

Abstract

Semiconductor devices, and in particular InP-based laser devices, are usually bonded on a mounting plate (called a submount or heatsink) or directly onto a package. This bonding assembly, which comprises the die-bonding metallic layers, the joint solder and the submount, serves the purpose of heat dissipator, mechanical support and electrical conductor. As such, the quality of both the bonding metallization and the submount are as important as the device die itself to assure the short- and long-term reliable operation of the electronic assembly. Due to its high thermal conductivity, diamond has been used as a very efficient thermal conductor and dissipator under electronic and photonic devices. This application has become even more attractive since the commercialization of the chemically vapor-deposited (CVD)-diamond, due to its lower cost and larger available surface area compared to natural diamond. Therefore it is only natural to use CVD-diamond as the material of choice for mass production of high-power InP-based laser diode submounts. The device is attached to the submount by a metallic bonding medium that contains a few layers, such as an adhesion layer (typically of titanium (Ti) adjacent to the submount), a barrier layer (typically of platinum (Pt)) and capped with hard solder (such as gold–tin (AuSn) eutectic alloy, which has a melting temperature of 278 °C). While offering optimum bonding conditions, the Ti/Pt/AuSn bonding system provides a high quality bond of the laser diode to the CVD-diamond submount. However, the extensive reaction of the AuSn solder with the Pt and Ti layers, even after short bonding periods of 5–10 s, may lead to mechanical deterioration of the bonded assembly, resulting in delamination of the metal and failure of the bond. This failure occurs mainly due to the thermodynamically reactive nature of the Pt–Sn couple, which reacts almost spontaneously even at room temperature. The reaction consumes the Pt layer and an appreciable amount of Sn, leading to the disappearance of the barrier layer and to dilution of Sn from the solder. The variation in the molten solder stoichiometry results in premature solidification of the solder through the bonding cycle after consumption of the entire Pt barrier layer, and dissolution of the Ti adhesion layer, as well. In order to maintain the good wetting performance of the AuSn solder to the Ti/Pt metals, but yet to improve the thermodynamic stability of the metallurgical bonding system, various other metals such as Ni, W, Cr and some of their alloys were evaluated as advanced alternatives to the Pt barrier layer. The quality of the evaluated metallurgical systems was judged upon wetting performance, thermodynamic stability and lack of premature freezing of the molten solder. The Ti/W/W(Ni_3Sn_4)/Ni_3Sn_4/Au multilayered structure was finally defined as the optimal and superior metallurgical scheme for the purpose of bonding laser chip to CVD-diamond submount. The time required until the first surface local freezing phenomenon was observed at the AuSn solder (with eutectic composition of 80 wt.% Au) on Ti/W/W(Ni_3Sn_4)/Ni_3Sn_4/Au structure while melted at 320 °C was 200 s, compared to 5–10 s at the Ti/Pt/Au/AuSn system. At the former system the solder was maintained melted at 320 °C for more than 1 h before it was completely frozen, which is much longer than the 30 s measured for the latter system. It was also observed that not only did the AuSn solder on the Ti/W/W(Ni_3Sn_4)/Ni_3Sn_4 multilayer maintain its accurate stoichiometric composition through the entire bonding cycle, but it also provided excellent adhesion and integrity for the entire bonded assembly.

Introduction

An InP laser diode is typically bonded to a submount that provides mechanical stability, heat dissipation and electrical connections to one or more electrical sources. A reliable device bonding is essential to provide short- and long-term operating reliability. The quality of the bonding medium depends on the appropriate selection

0254-0584/94/$07.00 © 1994 Elsevier Sequoia. All rights reserved
SSDI 0254-0584(93)01336-2

of the submount material, the solder metallurgical system, the barrier metallization scheme and the bonding conditions.

Submounts for laser devices have traditionally been manufactured from Si or ceramic materials such as BeO. Recently, due to its desirable high thermal conductivity and high electrical resistivity, diamond has been revealed as an attractive alternative for the submount material of choice, and in particular for operation of devices under extreme conditions [1, 2]. Thus, a natural application of diamond is likely to be one that takes advantage of its potentially high thermal conductivity, which can be as high as 25 W (cm °C)$^{-1}$ (at room temperature). This is about five times better than any other excellent conductors such as copper [3, 4]. Because of its high thermal conductivity, natural diamond has been used for many years as a 'heat sink' or thermally conducting substrate for dissipating heat from electronic and photonic devices. The demand for such substrates formed an obvious market for new chemically vapor-deposited (CVD) diamond material, which potentially has the advantages of lower price and larger available processing surface areas. This potential as a passive electronic component, has been featured in all the reviews that assessed the future of CVD diamond. American Telephone & Telegraph (AT&T) Co. has recently announced [5, 6] the first commercial application of CVD diamond as submounts for InP-based laser devices, and it is expected that this concept will be applied in a wide range of electronic and photonic devices.

Traditionally, solder preforms, paste or deposited solder have been used to bond microelectronic and photonic devices onto submounts. The deposited solder, however, provides significant advantages over other techniques, such as decreased oxide formation prior to the initiation of the bonding cycle, and more accurate control of the bonding media thickness and volume [7]. The few commonly-used solders are the lower-melting elements such as In (183 °C), medium-melting systems, such as binary Pb–Sn alloy (223 °C), and higher-melting alloys, such as AuSn (278 °C), AuGe (361 °C) or AuSi (364 °C). Generally, the lower-melting solders exhibit better thermal conductivity but are mechanically weaker, compared to the higher-melting solders. Thus, for better thermal stability and improved long-term reliability of performance, use of the higher-melting solders is preferred [8–11]. Au–Sn solder has been widely used in optoelectronic applications due to its high, but practical, melting temperature, which allows for efficient bonding of devices that also contain temperature-sensitive elements such as Au-based contacts.

The Au–Sn phase diagram is a eutectic binary phase diagram (as shown in Fig. 1(a)), with two eutectic melting points, at 80 wt.% Au (278 °C) and at 90 wt.% Sn (232 °C). The former composition was used for the above-discussed soldering applications and is defined by very steep liquidus lines on both sides of the eutectic melting point. This means that, for example, enriching the eutectic composition by 1 wt.% of Au leads to an approximately 30 °C increase in the melting temperature. Thus, it suggests that the AuSn solder system requires very accurate process control of both the solder composition and the bonding temperature to permit successful bonding.

The third important factor involved in the bonding assembly includes the adhesion-barrier metals that allow for efficient introduction of the AuSn solder onto the submount. The commonly-used adhesion-barrier metals are the Ti/Pt metals, which have been widely studied and reported [10, 12].

It was reported that introducing AuSn solder onto the Ti/Pt adhesion-barrier metal structure leads to a rapid and extensive metallurgical interaction between the Sn and Pt to form certain intermetallics, such as PtSn [13]. The binary phase diagrams for the elements comprised in the Ti/Pt/AuSn metallurgical scheme are provided in Fig. 1, and further discussion on the thermodynamics of these systems is available in the literature [7, 10, 14, 15]. The reactivity of these systems results in intensive reactions that take place at the Ti/Pt/AuSn interface. The most disturbing one is the consumption of the Sn from the solder overlayer, which leads to the formation of an Au-rich solder layer, and results in elevation of the solder melting temperature and its premature freezing through the bonding cycle.

Thus, the complex nature of the AuSn solder system combined with the fact that SnPt is such a reactive system, suggest that the overall Ti/Pt/AuSn bonding metallurgical system is relatively unstable, and although being used, only a narrow bonding processing window is available. As a result, studies have been initiated to explore some potential metal alternatives for the solder and for the barrier metal systems, in order to achieve a more robust and stable bonding process. The initial, and simplest approach is to replace the reactive Pt barrier layer with a more stable metal, as is shown schematically in Fig. 2.

Ni was found to be one of the more attractive candidates to replace the Pt barrier metal, for the following reasons. The Au–Ni phase diagram [16] (see Fig. 3(a)) suggests that the solubility of Ni in Au at temperatures below 350 °C is very limited. Au and Ni do not dissolve in each other at temperatures lower than 100 °C, and in addition Ni, as opposed to Pt, dissolves in Sn-based solders at very slow rates [17, 18]. However, some Ni-based intermetallics such as Ni_3Sn_4 and Ni_3Sn_2 [19–22] may still be formed during the bonding cycles at temperatures higher than 250 °C. Both intermetallics are stable and do not consume much

Fig. 1. Binary phase diagrams of the (a) AuSn, (b) TiPt, (c) AuPt, (d) PtSn systems.

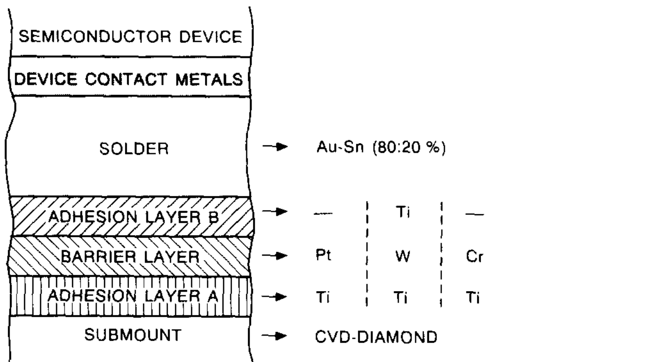

Fig. 2. Schematic presentation of conceptual design of simple bonded device assembly.

Sn (see Fig. 3(b)). In addition, pure Ni possesses superior thermal and electrical conductivities [23] compared to other potential barrier metals, such as Co or Pt. For these reasons Ni has, indeed, already been suggested as a barrier metal under the PbSn (95% Pb) solder [24].

Other metals that seem attractive as a replacement to the Pt barrier layer, are W and Cr. The binary phase diagrams of Au–W, Au–Cr and Cr–Sn (shown in Figs. 4(a), 4(b) and 4(c)) are given for reference, to be compared to the earlier-discussed Pt–Au and Pt–Sn systems, demonstrating the superior thermodynamic stability of the W- and Cr-containing systems. Unfortunately, no phase diagram is available for the Sn–W system, but the solubility of W in liquid Sn was reported to be very low ($\sim$0.001 at.%) even at 2000 °C, and no intermetallics were found in this system.

By replacing the Pt barrier metal layer with any of the above-mentioned alternative metals, better thermal stability of the bonding metallurgical system was, indeed, achieved. Cr was found to be less reactive than Pt.

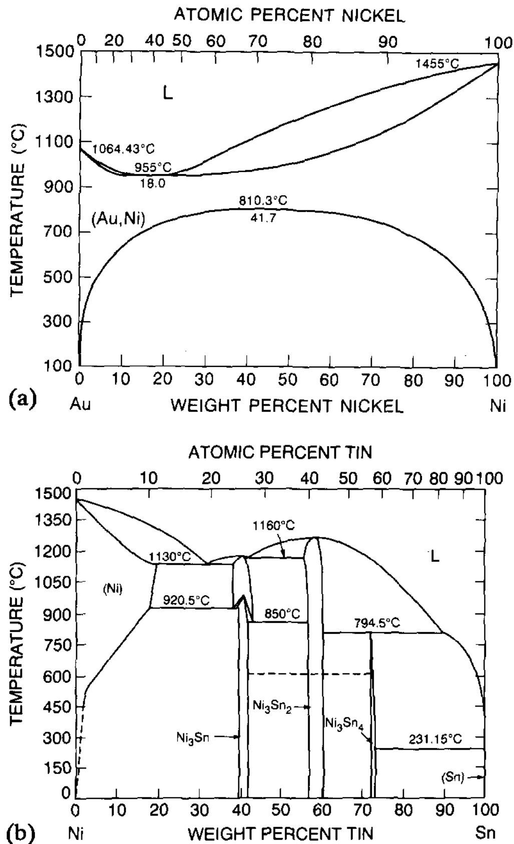

Fig. 3. Binary phase diagrams of (a) AuNi, (b) NiSn.

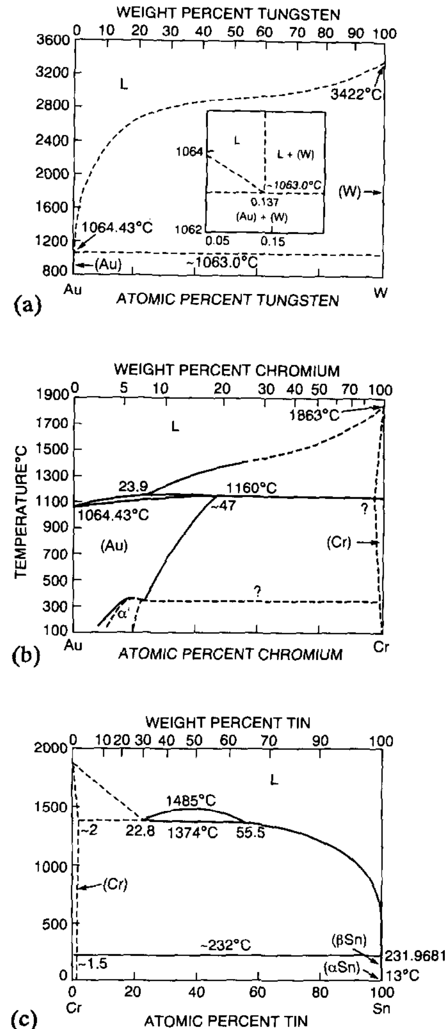

Fig. 4. Binary phase diagrams of (a) AuW, (b) AuCr, (c) CrSn.

When heated in contact with AuSn, Ni exhibited limited mutual solubility with the Au-based solder, and W provided a completely inert barrier under AuSn solder. The latter guarantees excellent thermodynamic stability of the system (see Fig. 2), but results in very poor adhesion between the AuSn solder and the W layer. Generally, the more inert the metal/metal interfaces, the better the thermal stability, which allowed for a wider bonding processing window and eliminated the premature freezing of the solder as a result of deviation from the eutectic stoichiometry composition. However, the most stable interfaces did not allow the formation of intermetallics, and thus resulted in poor adhesion of the metals as a result of lack of chemical bonding.

In an attempt to improve, for example, the W/AuSn interface integrity, a thin Ti layer (10 nm) was introduced between the W layer and the AuSn solder [25] (see Fig. 2). The adhesion in this case was improved, but the inert nature of the W/AuSn interface was degraded, and again led to premature freezing of local solder spots on heating at 350 °C, even after 15 s.

Thus it was concluded that adhesion of AuSn solder to W in the Ti/W/AuSn system can be further improved without causing wider interfacial reactions, simply by introducing a better-designed wetting layer between the W and AuSn layers. Thus a wide range of Ti/W_xM_y/AuSn systems was studied, in which M represents a metal that can potentially be alloyed with W to provide a sufficient wetting layer. In particular Ti/$W_z(Au_xSn_y)$/AuSn and Ti/$W_z(Ni_xSn_y)$/AuSn systems were examined. The adhesion of the solder to the barrier metal improved, and the most stable performance was observed with a W/W(Ni_3Sn_4)/Ni_3Sn_4 multilayer structure under the AuSn solder. Initial solder local freezing on heating at 320 °C required more than 3 min, and more than 1 h at this temperature was needed to completely freeze the entire 3 μm AuSn layer. In addition, an excellent solder-to-metal interfacial integrity was observed during and after the bonding cycle.

This paper reviews the procedure for developing a superior bonding metallization scheme which allows stable and reliable bonding of laser diodes to any type of supporting submount, and in particular to a CVD-diamond submount, using a high-melting AuSn solder.

Experimental

The diamond films used in this study were nucleated and grown on metal substrates by microwave-enhanced plasma chemical vapor deposition at 1.45 GHz. Depositions were carried out using a gas mixture of hydrogen, hydrocarbon and oxygen-bearing precursor, which resulted in an optically transparent CVD film. Except for some modifications in growth times, which led to changes in the CVD-diamond plate thickness, the deposition conditions were held constant from sample to sample. The self-supporting CVD-diamond plate was then chemically removed from the substrate. The plate surfaces were subsequently polished to mirror finish, metallized and laser-diced to heat-sink dimensions of about 0.65×1.25 mm with thickness of about 0.25 mm. These CVD-diamond films had a thermal conductivity in the range of 11–25 W (cm °C)$^{-1}$.

An adhesion layer of 100 nm Ti was DC-magnetron sputtered onto the mirror-finished CVD-diamond plates, followed by deposition of 200–500 nm of Pt, Ni, W or W-based alloy. AuSn solder was electron-beam evaporated onto these base metal layers in a multilayer structure to provide an AuSn stoichiometric eutectic (Au 80 wt.%) composition (T_m=278 °C) [26], at a total thickness of about 2.5–3 μm. The structure that was found to give the best results included an Au layer (0.5 μm) deposited onto the barrier layer, topped with four pairs of alternating Sn(0.35 μm)/Au(0.2 mm) layers, and covered with a final layer of Au(0.5 μm).

InP-based laser devices were then bonded to the metallized CVD-diamond submounts during thermal cycles of 320–350 °C for 5–10 s. The strength of the bond was assessed by shearing the device from the submount and analyzing the exact ruptured interface.

In other samples the bonding cycles were simulated by carrying out reflow heating cycles at conditions similar to the bonding cycles. The metallurgical systems were reflowed by introducing the sample onto an electrical heating plate in a covered quartz vacuum chamber, in order to allow for visual tracking of the melting and freezing phenomena of the metals. A stereomicroscope with 30× magnification was used to visually track any solder surface changes of the samples during the reflow process. The reflow process was carried out as follows: After evacuating the chamber to 5 mtorr for 2 min, forming gas (85% N_2, 15% H_2) was flowed into it at a constant flow rate. After complete purge of the chamber (about 2 min of gas flow), the heating plate was turned on, and the metallized samples were heated to temperatures in the range of 300–350 °C at a rate of 4.5 °C s^{-1}, as shown in Fig. 5. When the sample temperature reached 100 °C, timing was begun (t=0 s). Once an initial surface local freezing phenomena was observed, the elapsed time was recorded and defined as the 'surface local freezing time' (SLFT). After six more minutes of reflow, the power to the heating plate was turned off and the sample was cooled to room temperature. Some samples were maintained at the soaking temperature till the entire solder solidified. This time was also recorded, and defined as the solder 'global freezing time' (GFT).

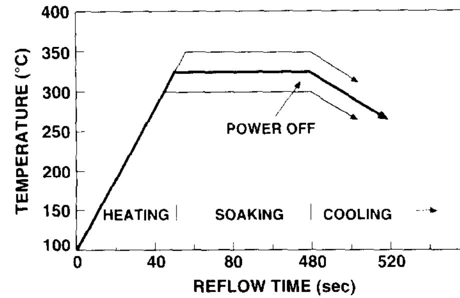

Fig. 5. Typical temperature–time profile of a reflow cycle under forming gas.

In addition to the reflow under forming gas, the samples were treated under flux (PEG400–5% abietic acid) in a simple bath furnace in order to evaluate the relative wettability of the different barrier metals to the AuSn solder in the temperature range 320–350 °C, for durations up to 5 min.

Composition and microstructural analysis of the different metallurgical samples were performed by a variety of means. Auger electron spectroscopy (AES) was used to obtain information on surface impurities (such as tin oxides) and, in conjunction with sputter depth profiling, to study the reaction of the adhesion and barrier metal layers with the AuSn solder through various reflow and bonding cycles. Rutherford back-scattering spectrometry (RBS) was used to measure the solder composition and thickness in the as-deposited and annealed layer structures. Scanning electron microscopy (SEM) was used to obtain microstructural information, both of the solder pad surface morphology (in plan view), and of the quality of the layers and interfaces, obtained by cleaving the sample under the solder pad and examining the cross-section. Optical microscopy provided a quick way to screen surface morphology. Differential scanning calorimetry (DSC) experiments were conducted using a Perkin-Elmer DSC-4 apparatus. Samples of 2–10 mg were analyzed in aluminum pans previously coated with carbon. The DSC samples and chamber were flushed with ultrahigh purity nitrogen gas, and subsequently the samples were heated at a rate of 10 °C min^{-1}.

Finally electro-optical analysis of bonded laser diodes was carried out to ascertain the final laser performance and the influence of the various metallurgical schemes on its performance.

Results and discussion

Ti/Pt/AuSn bonding scheme

Optimized AuSn solder structure

Currently, the AuSn soldering system is the most commonly used for high temperature bonding of high-power electronic and photonic devices. Bonding of the InP-based laser diode to the CVD-diamond submount is an excellent example of the use of this system.

It was concluded that sufficient bonding of the laser device to the diamond submount is achieved with a eutectic AuSn layer (Au 80 wt.%) with total thickness of 3 μm or less, in order to guarantee a sufficient thermal conductivity through the solder joint, and eliminate technical problems associated with the presence of excess solder on the device. Given the unstable nature of the Pt/AuSn metallurgical system, a number of AuSn solder multilayer structures with the required stoichiometric average composition and thickness were investigated in order to determine the system that gave the best bonding results [27].

Bonding is carried out through a rapid thermal cycle, in which the temperature is quickly ramped up to 320–350 °C and turned off in a period of 5 s. Clearly, differences in solder layer structure will affect the kinetics of the melting and bonding process, so that over the short time of the bonding process, different layer structures will lead to different results. For longer melting times (greater than 15 s), thermodynamic considerations become important. Then, no matter what the initial as-deposited solder structure may have been, the behavior of the melt over time will depend on the initial Au, Sn and Pt average ratio, since at this point, being the main interacting species, they have probably reacted completely. Presumably, the Pt barrier layer will consume an appreciable amount of Sn from the AuSn solder to form PtSn species. This has the detrimental effect of destroying the Pt barrier layer and altering the AuSn composition so that the melting behavior is adversely affected.

The optimal metallization structure should allow a significant portion of the Pt barrier to remain intact during the bonding step, with the AuSn solder remaining molten long enough to allow for the bonding of the laser device. Note that the optimal metallization structure depends critically on the time scale of the bonding process.

The effect of the AuSn solder layer structure on bonding properties is demonstrated through the evaluation of two samples. In the first sample (referred to hereafter as Sample I), a simple three-layered Au(0.8 μm)/Sn(1.14 μm)/Au(0.8 μm) structure was deposited on top of the Pt/Ti barrier metals. This represents a simple processing sequence, with only two metal interfaces within the solder. The second sample (referred to hereafter as sample II) contains nine Au/Sn alternating layers, produced through a relatively complicated processing sequence. Both samples were prepared with the same overall thickness and Au:Sn ratio. In both cases 0.5 μm of gold was deposited directly on top of the Pt layer in an attempt to separate the Sn and the Pt, and thus minimize the Sn–Pt interreaction. Each as-deposited sample was cut into several pieces to be processed at different temperatures. Two annealing conditions, 320 °C for 5 s and 320 °C for 10 s, were applied, and the results were analyzed and compared to the as-deposited sample properties.

RBS data of the two samples were used to determine the solder composition and thickness. The data for the as-deposited sample and for the sample annealed at 320 °C for 10 s are summarized in Fig. 6. Interpretation of the as-deposited samples data shows that the overall thickness and Au:Sn composition of samples I and II were quite similar. The total thickness in both cases was about 2.7 μm, and the average Au:Sn ratio was close to 80:20 wt.%. Differences in the Au:Sn ratio with depth were observed between the two as-deposited samples, which was expected due to the different methods of preparation. For both as-deposited samples, the RBS data shows that no layers of pure Sn existed even after the deposition process. The general shape of the spectra confirms the existence of a predominantly pure gold layer at the bottom of the solder next to the Pt, and another Au layer on top of the solder. In the middle, the Sn intermixed readily with the gold to form an approximately 50:50 at.% alloy. The middle layer composition varies between samples I and II. In general, the picture that emerges is that during deposition, the first gold layer goes down on top of Pt and forms a sharp interface. The next layer deposited, which is Sn, is known to form a fairly porous layer. When the next Au layer is deposited onto it, it mixes readily with the Sn to form an AuSn alloy. The process continues in this manner until the final gold deposition, which is a fairly thick layer. Some portion of that may react with the previously deposited Sn layer, leaving a portion of mainly pure Au on top of the structure.

After annealing, the RBS spectra from samples I and II are qualitatively different. Note that the analysis beam spot size used here is ~250 μm in diameter, which covers most of the solder pad. Any lateral variations in thickness and composition will be averaged in the final spectrum. The data from sample II (Fig. 6(b_2)) show a final solder composition of 80:20 wt.% and a fairly uniform thickness of solder over the pad. In contrast, the data from sample I (Fig. 6(a_2)) show a similar solder composition but a greatly smeared low energy edge. This indicates very nonuniform solder thickness across the pad, and hence a nonuniform melting behavior across different areas of the pad.

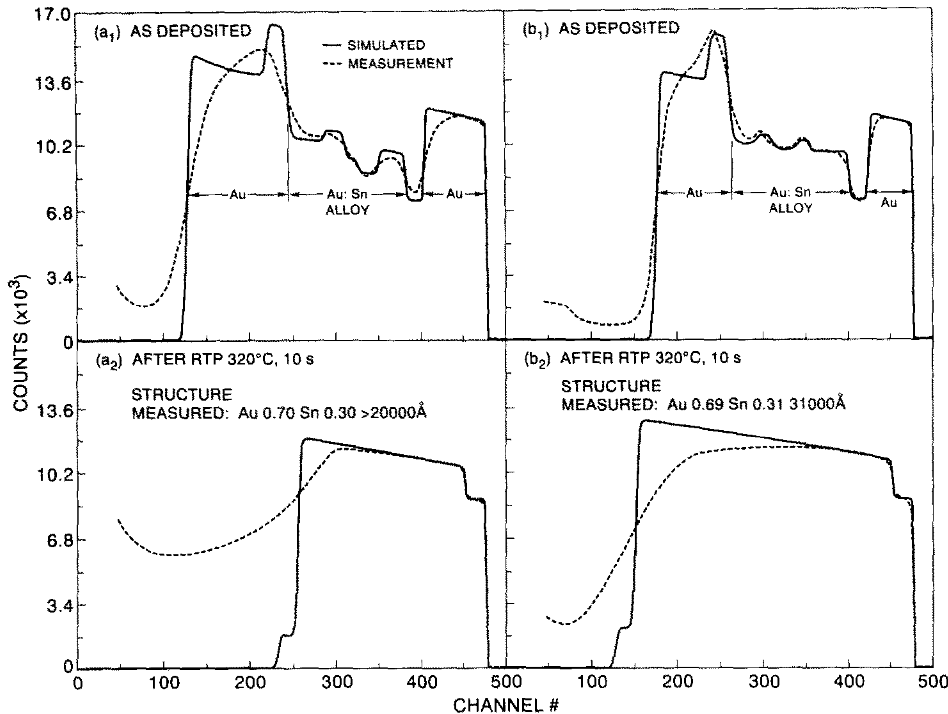

Fig. 6. RBS spectra of metallized submounts; (a_1) and (a_2) are as-deposited and annealed spectra from sample I (simple 3-layer structure); (b_1) and (b_2) are as-deposited and annealed spectra from sample II (9-layer structure). See text for deposition details.

Figure 7 gives SEM cross-sectional micrographs from as-deposited and annealed (320 °C 5 s) pieces from samples I and II. The microstructural information obtained from the SEM photos clearly shows the differences between samples I and II and the reason for the different melting behavior. The cross-sectional micrograph from sample I, which was the simple structure, shows the individual Ti, Pt, Au and Sn layers quite clearly. Note that within the solder layer the original Au/Sn/Au interfaces are separated in certain regions. From the RBS data, we know that, on average, the middle portion consists of 50:50 at.% Au–Sn with pure Au layers on top and bottom. Perhaps due to the greater strain present in the much thicker layers used in sample I, or to a volume change in the layer during formation of the AuSn alloy, empty spaces and gaps occurred in several places within the solder layers of sample I. This is in contrast to the more complex layering used in sample II. In that case, the SEM micrographs show closely packed layers of Au and Sn with no gaps or separations at any of the interfaces. On the basis of this information, the difference in melting behavior of the two samples is easily understood. For sample II, the uniform layering of Au and Sn leads to uniform melting of the solder which, during the 5 s of melting, forms a final layer of Au:Sn 80:20 wt.% solder which has uniform thickness throughout the area of the pad. On the other hand, in sample I, the gaps observed in the solder mean that during a short 5 s annealing, there is not enough time for uniform mixing of the AuSn solder, and this leaves areas that are either gold-rich or tin-rich. Since the melting is nonuniform across the pad, areas of different thickness are formed, which greatly differ in their local composition.

This nonuniformity in melting for sample I is most easily observed in the SEM plan view photos shown in Fig. 8. The dendritic structures found after the melting of sample I are thick regions which are shown to be gold-rich by EDS analysis taken *in situ* by SEM. A notable difference in the feature size is observed depending on the reflow duration, as is demonstrated in the comparison of the 5-s and 10-s melted samples in Fig. 8. The premature resolidification of these localized features was observed in this case even after only 2–3 s of melting at temperatures above the eutectic melting point, and is consistent with the gold-rich composition as observed by SEM. In contrast to this sample, the plan view photo of sample II after melting shows a uniform surface morphology across the pad.

Thus, it is concluded that a multiple-layered structure consisting of thinner Au and Sn layers is superior to a simple thick three-layered structure, with respect to melting behavior during bonding. The main reason is that a higher degree of strain and volume change occurs in the simple structure which produces gaps in the interfaces of the solder layer. During the bonding cycle, these gaps interfere with uniform melting behavior and

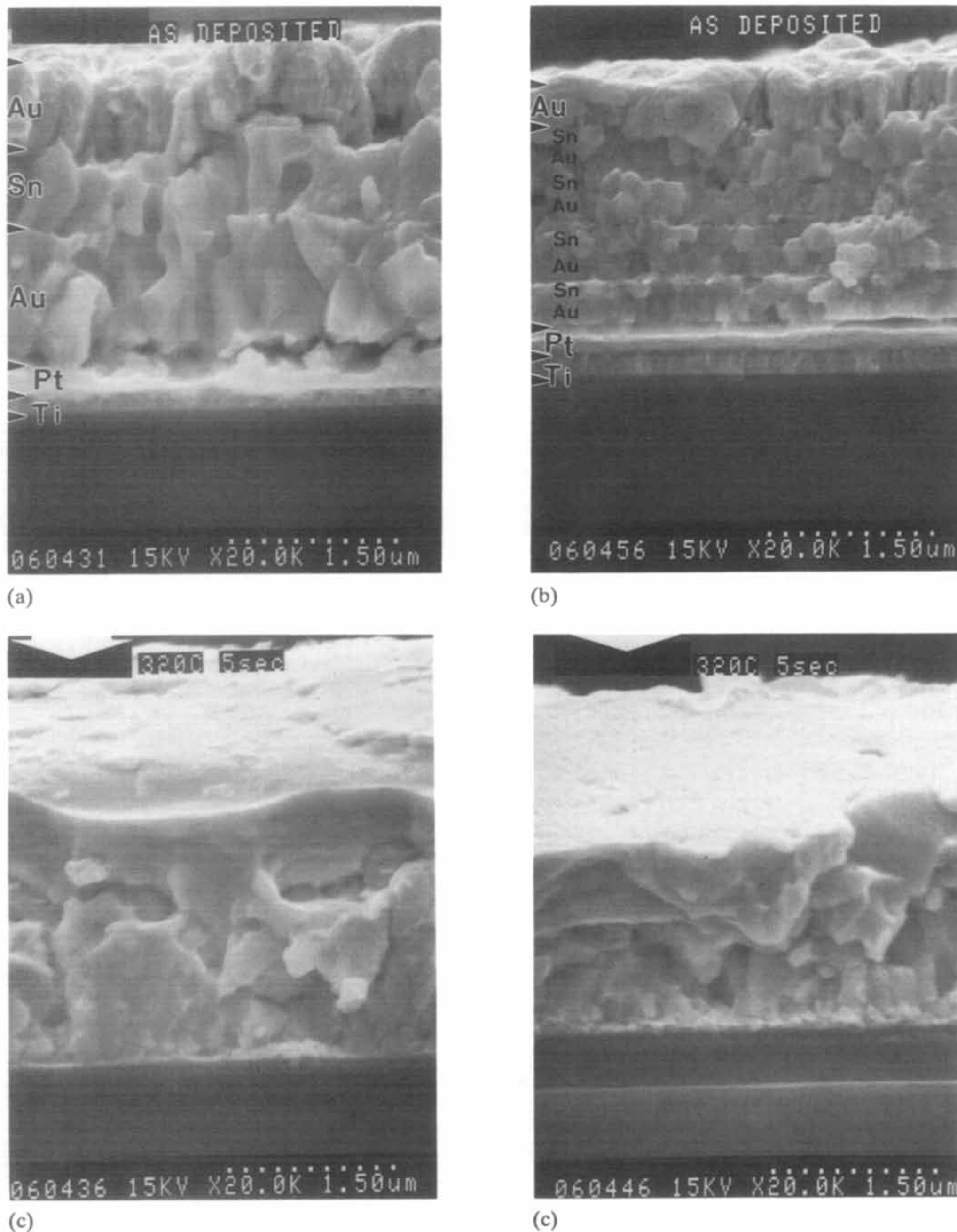

Fig. 7. SEM cross-sectional micrographs of a metallized Au(0.8 μm)/Sn(1.4 μm)/Au(0.8 μm)/Pt(0.2 μm)/Ti(0.1 μm) submount, (a) as-deposited, and (b) after a bonding cycle at 320 °C for 5 s, and of a metallized Au(0.5 μm)/(3×)/Sn(0.35 μm)/Au(0.2 μm)/Au(0.5 μm)/Pt(0.2 μm)/Ti(0.1 μm) submount, (c) as-deposited, and (d) after a bonding cycle at 320 °C for 5 s.

create localized areas of Au-rich solder which freeze prematurely.

AuSn–Pt interactions

During a 5 s annealing, interaction of Sn with the Pt layer does not adversely affect the bonding process, especially if the as-deposited structure has a layer 0.5 μm or greater of pure gold directly in contact with the Pt. AES spectra on specially-deposited test structures were obtained to determine how much of the Pt barrier layer would be consumed during the typical bonding times of 5–10 s. These data are shown in Fig. 9. Basically, it shows that for short anneal times, Sn does tend to segregate towards the Pt interface, presumably to form Pt–Sn compounds, but that a significant amount of the original Pt layer is left intact during the bonding process. This does not mean that the Pt–Sn interaction is unimportant. As mentioned above, understanding of

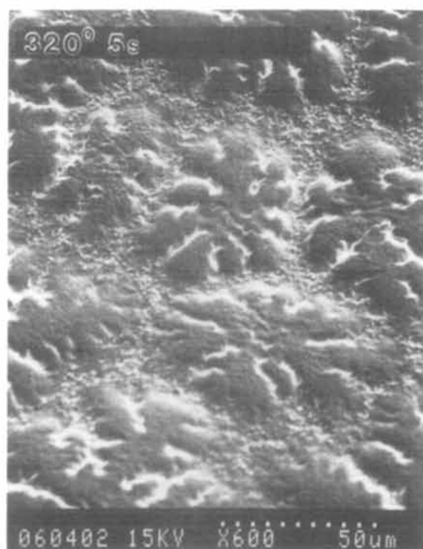

(a)

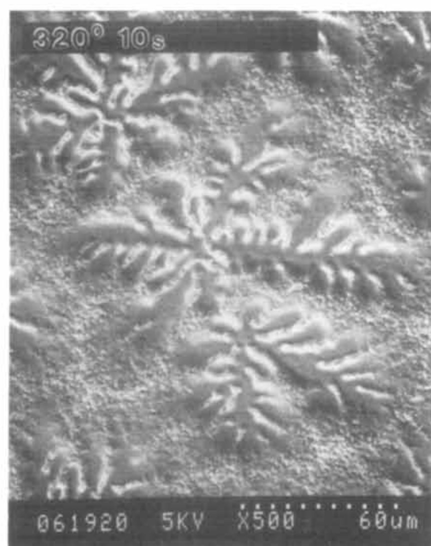

Fig. 8. SEM plan-view micrographs of a metallized Au(0.8 μm)/Sn(1.4 μm)/Au(0.8 μm)/Pt(0.2 μm)/Ti(0.1 μm) submount after bonding cycle at 320 °C for (a) 5 s, (b) 10 s.

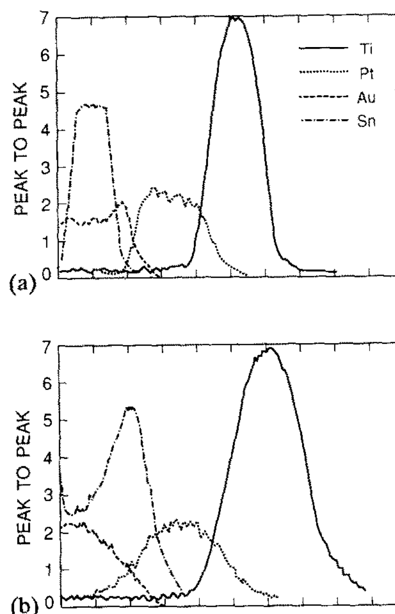

Fig. 9. Auger spectra of structure with Au(0.2 μm)/Sn(0.25 μm)/Au(0.1 μm) solder deposited on Ti(0.1 μm)/Pt(0.2 μm) barrier metals. (a) As-deposited; (b) annealed at 320 °C for 5 s.

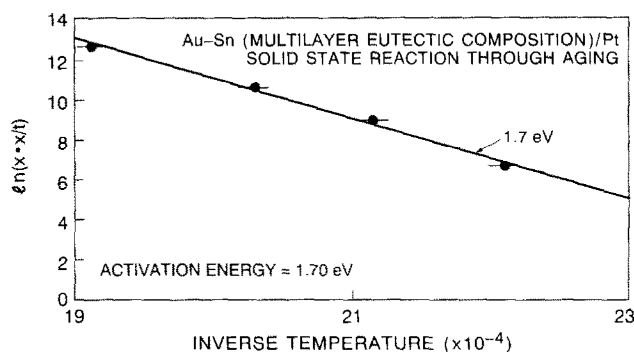

Fig. 10. Arrhenius plot of Sn–Pt reacted layer thickness squared divided by the reflow time for solid-state reactions vs. inverse temperature, at temperatures below eutectic melting point.

this interaction is very important for establishing and understanding the behavior of the metallization systems under more severe bonding conditions, and the long-term shelf life of the submounts and long-term reliability of the assembly under operating conditions.

Previously it was reported [14] that the AuSn–Pt reactions take place both in the solid state and at the solid–liquid interfaces. The activation energy for the mutual diffusion process in the solid state was determined to be 1.35 eV, for samples that had equal thicknesses of both AuSn solder and Pt film (about 300 nm each). In the standard bonding procedure, however, 3 μm of AuSn solder are deposited onto 0.1–0.2 μm of Pt, and in this structure, almost complete consumption of the Pt by the Pt–Sn interaction was observed after 10–15 s of AuSn melting throughout the bonding. The Pt–Sn reaction was found to be thermally activated and not self-limiting as long as the supply of Sn is not exhausted. According to recent studies [28], the Sn–Pt solid state interaction activation energy was found to be 1.7 eV (see Fig. 10). It was also found that the entire Pt layer (up to 0.4 μm thick) may be consumed at the processing temperature, during storage and through solder deposition steps. Once Pt reacts with AuSn to form the PtSn intermetallics at the Pt/AuSn interface, as well as dissolving into the molten AuSn solder to form a ternary $Au_xSn_yPt_z$ compound, it no longer acts as an effective diffusion barrier. Thus special attention must be paid to the thermal energy that is introduced into the Ti/Pt/AuSn metallization

system before, during and after the bonding cycle to eliminate these reactions. As a consequence of the complete consumption of Pt, Ti will have intimate contact with Au, which is well known to motivate extensive formation of intermetallics as a result of the reactive nature of the Au–Ti system. This may jeopardize the short- and long-term electrical, mechanical and thermal performance of the bonded assembly.

Further studies on the stability of the Ti/Pt/AuSn system were obtained by calorimetric (DSC) measurements of samples containing the above-described AuSn multilayer eutectic structures (3 μm thick), which had been deposited onto SiO_2 inert substrates and onto various thicknesses of Pt layers. Figure 11 provides a summary of this analysis. During heating of the AuSn/SiO_2 sample, a sharp peak is observed at 278 °C, which is the exact AuSn eutectic melting temperature. Having the correct eutectic composition results in a heat of transition of 8.7 cal g^{-1} through the melting reaction at 278 °C. Samples containing an AuSn layer on both the 50 nm and 100 nm Pt layers exhibited the eutectic melting endotherm superimposed on a sharp exotherm as well as a broad endotherm centered near 290 °C. There was also evidence of further endotherms in the temperature range 370–390 °C. When depositing the solder onto a 200 nm layer of Pt no endotherm corresponding to the eutectic transition is observed, but only a broad exotherm beginning at about 250 °C and a well-defined endotherm at 370 °C.

The exotherm that occurred at around the eutectic temperature was attributed to Pt–Sn reactions, which were found to be rapidly accelerated when the solder was molten. When sufficient Pt is present, this mixing takes place and can be observed even below the solder melting point, implying that a rapid solid state diffusion has occurred.

Once the DSC was completed, the samples were cooled to 200 °C and annealed at this temperature for 40 min, followed by secondary DSC cycles, as shown in Fig. 12. The samples that contained a relatively thin Pt layer (50 nm, 100 nm) still exhibited the eutectic transition at 278 °C, although with diminished intensity, reflecting the reduction in the total amount of AuSn eutectic compound as a result of the partial consumption of the Sn by the Pt–Sn interaction. The AuSn heat of transition has changed from an unperturbed value of 8.7 cal g^{-1} to 4.2 cal g^{-1} in the presence of a 50 nm Pt layer, and to 1.1 cal g^{-1} in the presence of a 100 nm Pt layer. Once a 200 nm layer of Pt was introduced under the AuSn solder, no melting transition was evidenced through the second DSC cycle at the solder eutectic melting temperature.The exotherms observed in the initial scans are not shown at any of the subsequent DSC studies, suggesting that the AuSn has been saturated by complete consumption of all the available Pt, and no eutectic melting reaction took place in this stage.

The DSC results further emphasize the major deficiencies of the Ti/Pt/AuSn bonding system. No matter how thick the Pt barrier layer, it will always be partially or fully consumed through both solid state Pt–Sn interfacial reactions, and by dissolution into the AuSn eutectic liquid, once heated to 278 °C. As a result, a two-fold problem arises. A complete loss of the Pt layer takes place, allowing for further intermixing of the Ti adhesion layer, initially adjacent to the submount, with the liquid Au–Sn–Pt, which eventually leads to delamination of the entire metallurgical system and mechanical failure of the bonded joint. In addition, the AuSn eutectic solder stoichiometry deteriorates as a result of dissolution of the Pt, and subsequently the Ti into it, and the solder freezes prematurely and cannot be

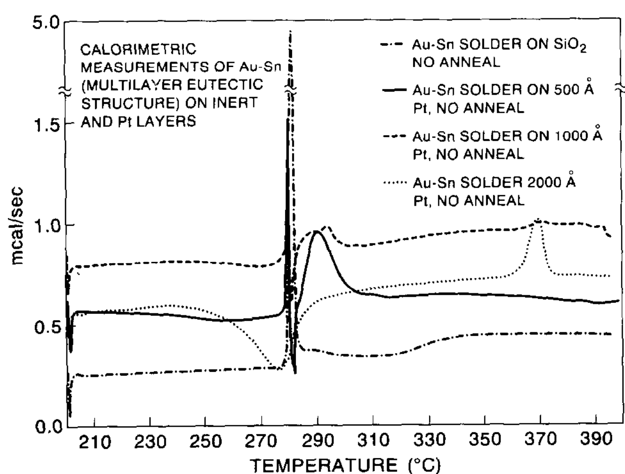

Fig. 11. DSC scan of AuSn solder film (3 μm thick) deposited onto SiO_2 and on Pt layers with various thicknesses.

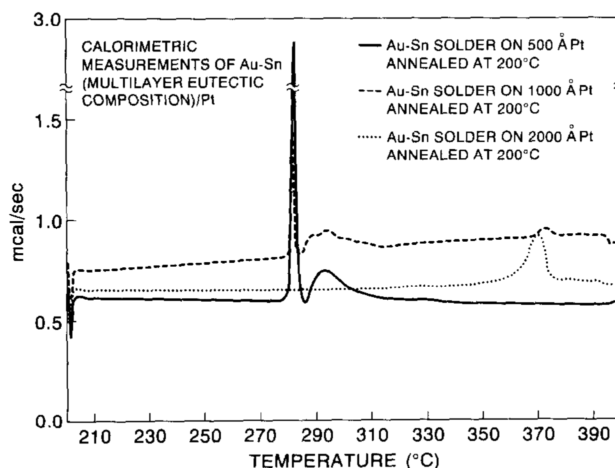

Fig. 12. DSC secondary scan of samples of AuSn solder films (3 μm thick) deposited onto Pt layers with various thicknesses, after annealing at 200 °C for 40 min.

remelted at the bonding temperature to permit a successful bonding process.

Based on the above, by executing the 5 s bonding cycle, we have established the multilayer solder structure as our commonly used solder for the purpose of bonding InP-based laser devices to CVD-diamond submounts. Figure 13 presents an optical micrograph of a metallized CVD-diamond submount (Fig. 13(a)), and of the same submount after bonding the InP-based laser device onto it, and shearing it off (Fig. 13(b)). The center metal geometry represents the Au–Sn multilayered solder bonding pad which is deposited onto the barrier Pt–Ti larger area of metallization. The Au–Pt–Ti areas on the right-hand side of this submount are used as a ribbon or wire bonding pad to connect the back side of the laser device to the submount, as well as the submount to the laser package. The InP-based laser device was bonded to the CVD-diamond submount in a junction-down configuration, using a thermal cycle of 320 °C for about 5 s. Figure 13(b) shows the almost complete dielectric and metal pattern of the front side of the InP-based laser device. One can conclude that the quality of wetting of the device to the CVD-diamond submount is excellent, leading to adhesion of almost 100% of the device front area to the submount. Thus, the shearing results in loss of adhesion in the semiconductor/metal interface comprised in the laser structure, rather than in the device metal/dielectric-solder interface, leaving the bonded metal, and dielectric films bonded to the submount, as observed in the micrograph.

Figure 14 presents an optical micrograph of an InP-based laser device bonded to a CVD-diamond submount which is then bonded to a BeO testing stud, as well as a schematic description of the structure. This bonded device configuration represents the state-of-the-art bonding technology in which an AuSn multilayered solder (3 μm thick) is used on top of Pt(200 nm)/Ti(100 nm) barrier metals adjacent to the CVD-diamond submount. This bonding configuration gave the InP-based laser device a superior bonding performance compared to the traditionally used bonding configurations, such as In solder on BeO submount. Improvements of up to 30% in the device rollover current, power dissipation and optical radiated light were observed, as partially illustrated in Fig. 15.

In summary, it is obvious that the combination of the complex nature of the AuSn solder system, and the fact that Sn–Pt is such a reactive system suggests that the overall Ti/Pt/AuSn bonding metallurgical system is thermodynamically unstable, and while being used, only a narrow bond-processing window can be explored to provide satisfactory results. Thus some studies have been initiated to evaluate potential alternatives for the solder and the barrier metal systems, in order to provide a more reliable and robust bonding process. The remainder of this review introduces a few of these alternative metals and metallurgical systems.

Ti/Ni/AuSn bonding scheme

Figures 3(a) and 3(b) present the binary phase diagrams of the Ni–Sn and Ni–Au systems, showing the potential for formation of few intermetallics through solid-state reaction in the first system, and the very inert nature of the second system. In addition the Ni, in contrast to Pt, dissolves into Sn-base solders at very low rates [13]. Thus, it appears that Ni would behave as a more suitable barrier metal than Pt between the Ti and the AuSn solder.

In order to evaluate the Ti/Ni/AuSn bonding system performance in comparison to the Ti/Pt/AuSn system two sets of similar samples from the two systems were

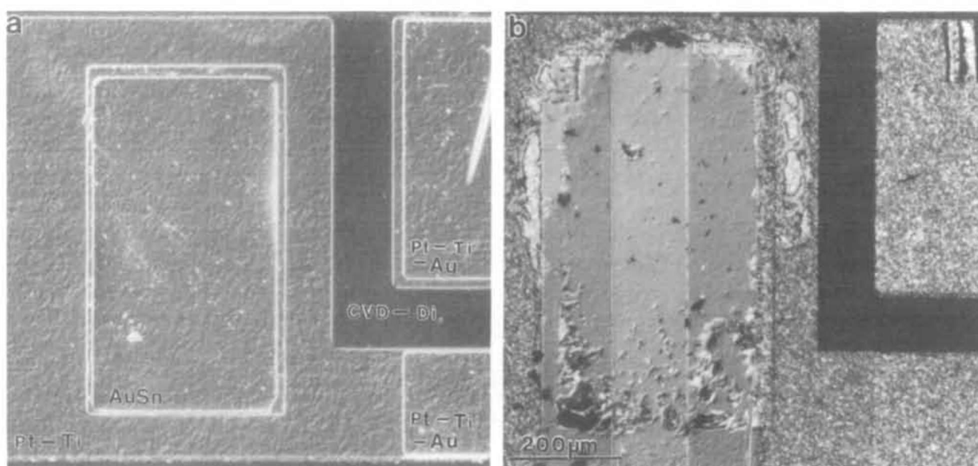

Fig. 13. Metallized CVD-diamond heatsink submount (a) as processed, and (b) after bonding InP-based laser device onto it and shearing it off (note the device's front side metal/dielectric film which was sheared off the device and left bonded to the submount).

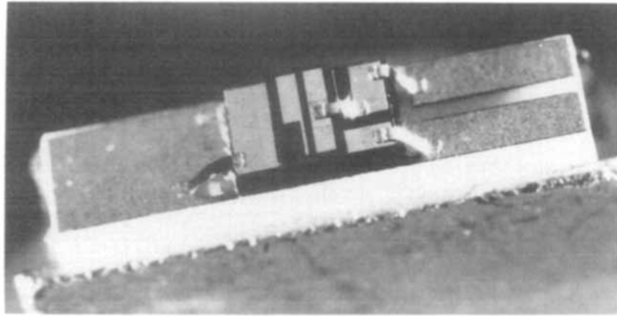
(a)

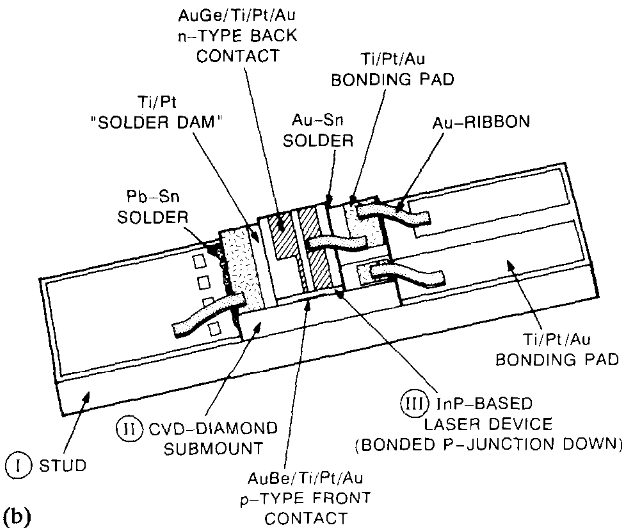

(b)

Fig. 14. Optical micrograph of an InP-based laser device bonded onto a AuSn/Pt/Ti metallized CVD-diamond submount on a BeO testing stud, and a schematic description of the configuration.

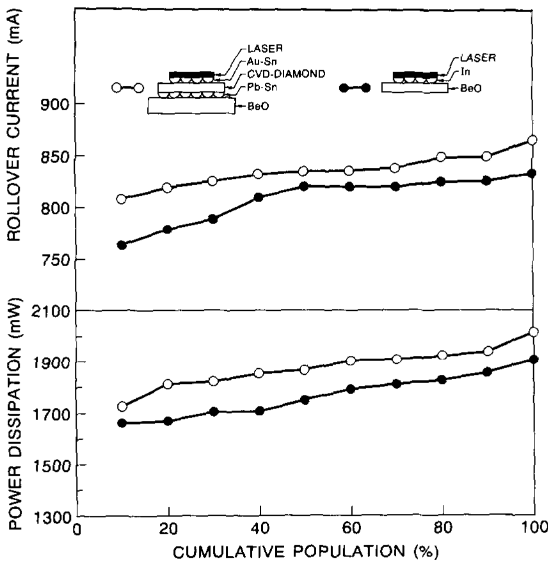

Fig. 15. Comparison of laser diode performance while bonded by AuSn solder to CVD-diamond submount, and while bonded by In solder to BeO submount.

prepared, containing similar Ti layers (100 nm thick) and layered structures of AuSn solder (3 μm thick). The Ti/Ni/AuSn samples showed longer SLFT and GFT than the Ti/Pt/AuSn samples. The Ti/Ni sample that was heated to 320 °C did not freeze completely before the power supply was turned off (a period longer than 60 s), while the Ti/Pt sample resolidified completely within 27 s after melting. Another set of comparable Ti/Ni and Ti/Pt samples was prepared, with structures of Ti/Ni(300 nm) and Ti/Pt(400 nm). These two samples possessed the same solder arrangement as shown in Fig. 7. The Ti/Ni sample had a nearly five times longer SLFT (45 s) than the Ti/Pt sample (9 s), showing that the molten state of the Ti/Ni/AuSn system was more stable than that of Ti/Pt/AuSn. SEM micrographs verified that the melted/solidified Ti/Ni/AuSn surface was much smoother than that of the Ti/Pt/AuSn system, as shown in Figs. 16 and 17 for the Ti/Ni and Ti/Pt samples, respectively. This suggests that the Ti/Ni/AuSn system should provide a better bonding platform than the Ti/Pt/AuSn system.

Figure 18(a) shows the AES depth profile of the Ti/Ni/AuSn as-deposited sample, which presents a limited interdiffusion between Au and Ni in the Au/Ni interface, whereas the Au and Sn in the solder have mixed completely even prior to reflow, as was previously reported [13]. After 1 min of reflow, a significant amount

Fig. 16. SEM micrograph of the surface morphology of a Ti/Ni/AuSn sample after reflow at 320 °C for 60 s.

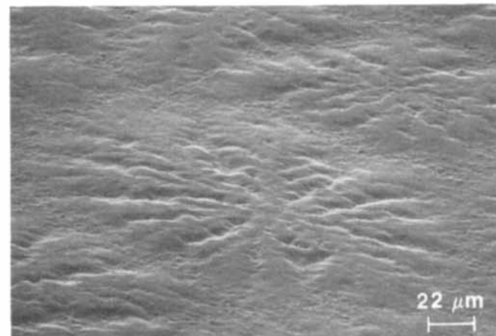

Fig. 17. SEM micrograph of the surface morphology of a Ti/Pt/AuSn sample after reflow at 320 °C for 60 s.

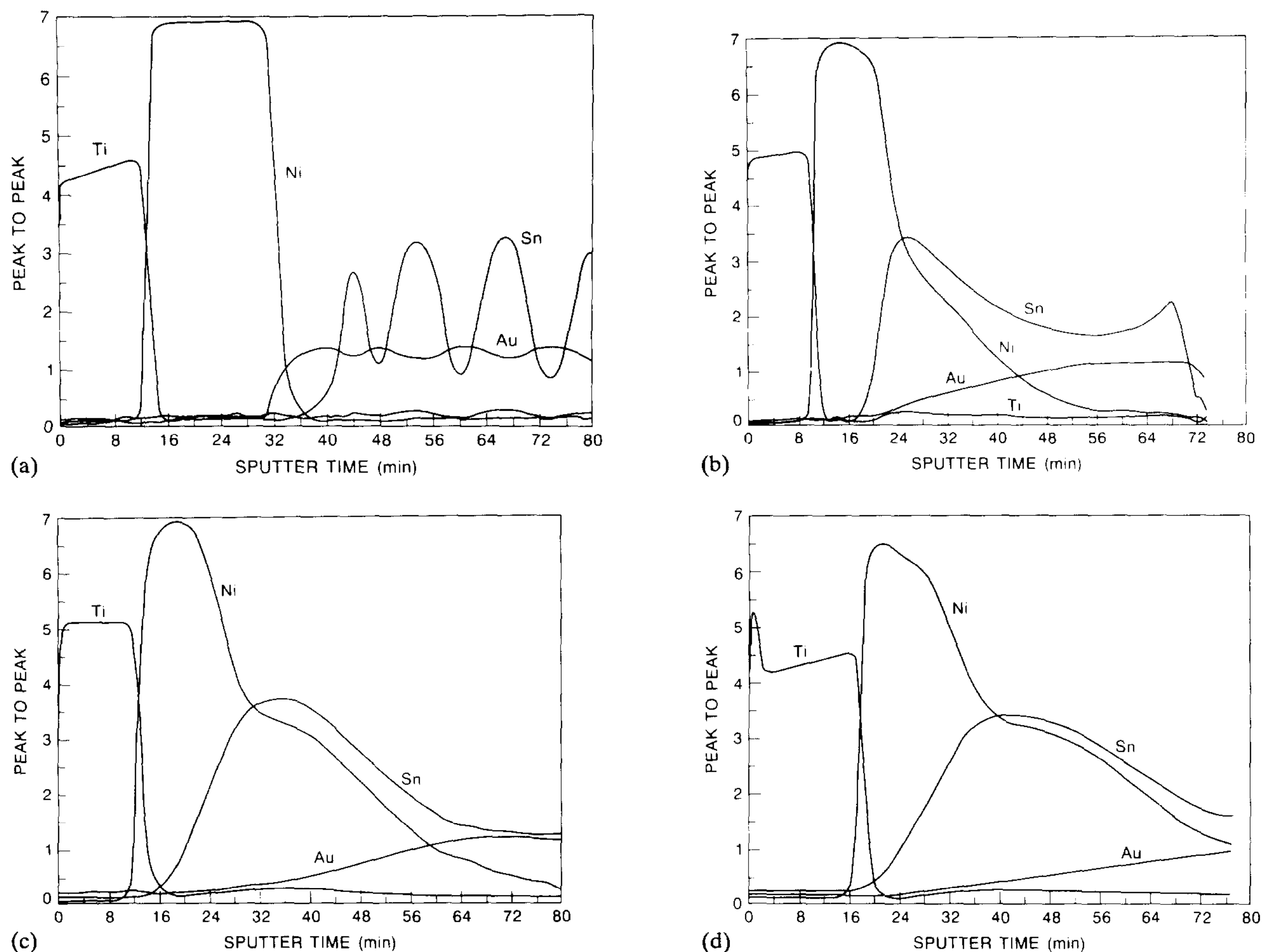

Fig. 18. AES depth profiles of Ti/Ni/AuSn structure (a) as-deposited and after reflow at 320 °C for (b) 1 min, (c) 3 min, (d) 5 min.

of Ni was dissolved into the molten solder. Only 100 nm out of the 300 nm of the original Ni layer remained after the reflow, as shown in Fig. 18(b). It is interesting to note that the Au did not diffuse as far as the Sn into the Ni layer. After 3 min of reflow, as shown in Fig. 18(c), about 50 nm of the pure Ni layer was still unreacted, however, with an observable limited migration of Au into the Ni. Au did not diffuse toward the Ti layer, as shown in Fig. 18(d). After two more minutes of solid state diffusion, Sn diffused almost all the way to the Ni/Ti interface, and only 25 nm of pure Ni remained unreacted after this duration of reflow. The penetration of Au into Ni layer was still suppressed. Thus, it is clear that Ni is a better barrier metal than Pt for prohibiting the migration of Au in this system.

From the above-discussed reactions that took place in the Ti/Ni/AuSn system, and from the earlier discussion about the reactions in the Ti/Pt/AuSn system, one can see that approximately the same thickness of Ni and Pt layers were dissolved by the molten Au–Sn solder during the first minute of reflow. A more severe premature freezing problem, however, was observed in the Ti/Pt/AuSn samples. It is thus clear that more Sn was consumed by the Pt than by the Ni, to form the related intermetallic compounds in the Ti/Ni/AuSn and Ti/Pt/AuSn systems, suggesting that the Ti/Ni/AuSn system is more thermally stable.

A mechanism to describe the reflow reaction kinetics, which comprises five major stages, is suggested:

(i) *Melting*: when the temperature of the solder exceeds 282 °C, the Sn starts to melt and Au is dissolved into the liquid Sn through the formation of the eutectic composition. Complete melting usually occurred before terminating the reflow heating cycle.

(ii) *Formation of intermetallic compound*: when the molten solder contacts the barrier metal, Ni or Pt, ternary related intermetallic phases (containing Ni or Pt, Sn and Au) are formed. Parameters such as the relative dissolution rates of Ni or Pt, Sn and Au, related intermetallic phases in the liquid Au–Sn solder, and the formation rates of the intermetallic compounds affect the residual amount of unreacted Ni. According to the AES results, once the ternary related intermetallic phases are formed, they might effectively retard the

dissolution rate of Ni into the melt due to their high stability at the reflow temperature.

(iii) *Solid state interdiffusion*: through the reflow process, intermetallic compounds keep forming and coalescing through intergrain diffusion mechanisms. In spite of the existence of stable intermetallic compounds, Sn and Au in the solder will still react with pure Ni after diffusing through the grain boundaries of the intermetallic compounds. At this stage, the diffusion rate of Sn and Au in these intermetallic compounds dictates the Ni consumption rate.

(iv) *Solidification of solder*: once the Sn has reacted with Ni, starting from stage 2, a local depletion of the Sn exists. According to the Au–Sn phase diagram, the freezing temperature of the AuSn solder increases by about 30 °C for every deviation of 1 wt.% of Sn from the eutectic Au–Sn (80:20) solder composition. Therefore, a local partial freezing always occurs as the Sn reacts with the Ni. When the concentration of the Sn in the solder drops below the eutectic composition, its melting temperature is higher than the pre-set reflow temperature, and solidification will occur at local sites, leading to subsequent total freezing of the solder.

(v) *Solid state interdiffusion of the various elements*: occurs with very low interdiffusion rates of the Sn from the solid solder to the base metal layers.

In conclusion, several major advantages were discovered from using a Ni barrier layer instead of Pt at the Ti/Metal/AuSn bonding metallization scheme. In particular, it was observed that Ni has better thermal stability during the soldering step compared to Pt, and therefore provided a longer freezing time (both local and global), and a final better reflow solder surface morphology.

It must, however, be emphasized that the Ni–Sn system, similar to the Pt–Sn system, is a very thermodynamically reactive system, and therefore the improvement in the thermal stability performance is not as significant as was expected. This conclusion motivated the search for more stable alternatives to the barrier metals of the bonding scheme.

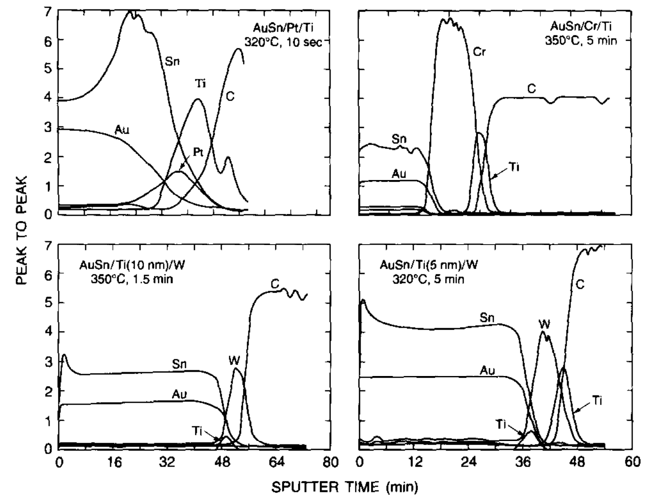

Fig. 19. Comparison of AES depth profiles from annealed submounts having four different metallization barrier schemes.

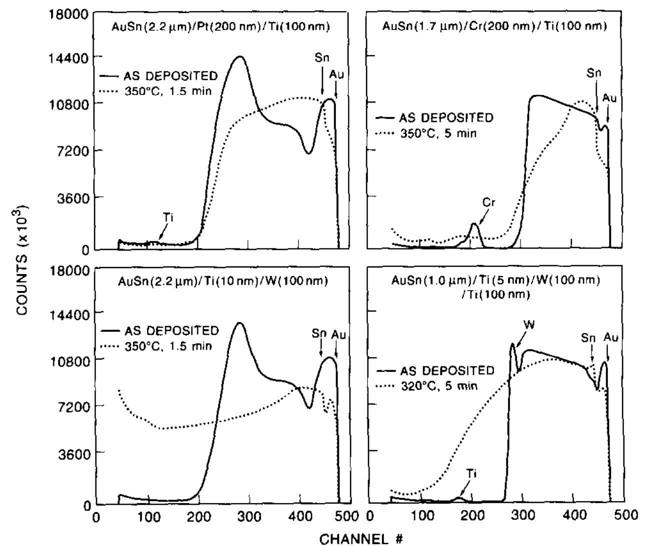

Fig. 20. Comparison of RBS spectra from submounts having four different metallization barrier schemes, as-deposited (——) and annealed (·····).

Ti/Cr/AuSn and Ti/W/AuSn bonding schemes

Based on the binary phase diagrams of Au–W, Au–Cr and Sn–Cr (unfortunately the Sn–W phase diagram does not exist), as shown in Fig. 4, both Cr and W seem to be very stable barrier metals and thus suitable to replace the Pt at a simple metallurgical bonding scheme.

The compositional stability of the CVDD/Ti/Cr/AuSn and CVDD/Ti/W/AuSn systems was studied using AES and RBS analyses. Representative data on the stability of the different barrier layers with respect to heat treatment is summarized in Figs. 19 and 20. The AES data shown in Fig. 19 gives concentration depth profiles for the various elements present in four annealed samples. These data provide information on the intermetallic reactions that occur between the solder and the various barrier metals. The RBS data is collected in Fig. 20 and shows both as-deposited and annealed spectra from four samples. The RBS data can be interpreted to give the average AuSn ratio and overall thickness of the solder on a particular submount. For reference, Figs. 19(a) and 20(a) show the AES and RBS data from a sample containing the standard Ti/Pt barrier metals, which are known to be reactive with the AuSn solder. Figures 19(b) and 20(b) show spectra from the specimen with the Ti/Cr barrier, and Figs. 19(c), (d) and 20(c), (d) show the data from the W/

Ti barrier (two different thicknesses of Ti wetting layer were investigated).

The AES data show a very clear difference between the behavior of the standard Pt/Ti barrier and the other two barrier metals after annealing. There are two obvious differences. First, the ratio of Au:Sn concentration changes dramatically with depth for the sample containing the standard Pt/Ti barrier, while in the samples containing either Cr or W barrier, the Au:Sn ratio remains constant throughout the depth of the material. Second, interdiffusion of Pt and AuSn is observed in the standard sample, whereas no interaction is detected between the barrier and the solder layers in the samples containing either the Cr or W barrier. In those samples, the Auger spectra show that the Cr and W layers remain inert to the solder at temperatures as high as 350 °C for melting times greater than 1 min.

These observations are, indeed, consistent with predictions based on the binary phase diagrams for these systems. Pt and Sn are known to form intermetallics, even at low temperatures. The behavior of the barrier in the standard sample reflects the propensity of Sn to react with Pt at the AuSn/Pt interface. This leads to a depletion of Sn from the top of the solder layer, while it tends to accumulate at the AuSn/Pt interface. At the same time, the integrity of the Pt barrier is degraded as PtSn compounds are formed in the interface region. On the other hand, neither Cr nor W are expected to form alloys with Sn or Au at the temperatures used in this study, and as observed, the interface between solder and barrier layers indeed remains sharp.

In the case of the W barrier layer, a very thin Ti layer of either 5 or 10 nm was introduced between the solder and the W layer to improve the adhesion between the solder and the W layers. After the anneal, the AES data shows that the Ti is still present at the solder/W interface, although it appears to have interacted mostly with the W layer.

In contrast to the W system, in the case of the Cr barrier, a Ti layer (100 nm thick) was introduced only between the Cr and CVD-diamond submount to improve the adhesion of the entire metal system to the submount. Some interactions were observed at the Cr/Ti interface resulting in the formation of Cr–Ti intermetallics.

The AES data for both Cr and W barrier schemes reflect stable metallization systems during heat treatments of 350 °C for as long as 5 min. This may suggest the advantage of using them to replace the Pt/Ti scheme in bonding InP laser diodes. It should be mentioned, however, that the typical bonding process is usually performed at lower temperature (about 320 °C) and for much shorter times (<30 s).

The main difference observed in the RBS data, shown in Fig. 20, between the standard sample containing the Pt/Ti barrier and the other samples containing Cr or W barriers is in the surface roughness of the solder layers after being annealed. For the standard Ti/Pt sample, the solder layer remains fairly uniform in thickness after the annealing. For that sample, the overall solder composition is about 77:23 wt.% Au:Sn, and the total thickness remains 2.25 μm after the anneal, with an estimated roughness of 0.1 μm. In contrast to this result, the samples with Cr or W barrier show greater solder roughness after annealing. For the Cr sample, the overall Au:Sn ratio is 79:21 wt.%, and the total thickness is about 1.7 μm after annealing with a roughness of 0.4 μm. The W samples show even greater roughness after annealing, and the solder layer appears to become thicker. For the W sample, the overall Au:Sn ratio was found to be 80:20 wt.%, and the total thickness increased from 1,8 to 2,5 μm after annealing, with a surface roughness of about 0.7 μm.

These RBS data indicate a potential problem with the wetting of the AuSn solder to more inert barriers, especially to W. The increased thickness and roughness of the solder layer surface measured after annealing is probably due to the tendency of the AuSn solder to 'ball up' on the W barrier layer as a result of surface tension and insufficient wetting. In the standard Ti/Pt system, the interaction of the AuSn solder with the Pt layer to form PtSn compounds at the interface is detrimental to the performance of the barrier layer, but actually improves the wetting of it, and thus the integrity of the system.

Figure 21 presents optical (100×) micrographs of the metallized CVD-diamond submounts that were used as heatsinks for the bonded InP laser diodes. The various metallization areas are detailed in the attached schematic for both the Ti/W/Ti system (Fig. 21(a)) and Ti/Cr system (Fig. 21(b)). These two submounts were reflowed at 350 °C for 5 min under H_2 (15%) N_2 (85%) ambient to study the stability of the bonding pad metallurgy during a long heat treatment at the bonding temperature. The same heat treatment applied to the standard Ti/Pt/AuSn system led to resolidification of the AuSn solder after 5–10 s as a result of the significant change in stoichiometry due to the reaction with Pt. In the Ti/W/Ti/AuSn and Ti/Cr/AuSn systems, the AuSn solder remained liquid throughout the 5 min reflow, providing clear evidence of the inert nature of AuSn on Cr or W barrier metals, as observed by AES. This long reflow process, however, led to the formation of a rough surface morphology containing pits and holes, in particular for the W/Ti system. It should be emphasized that when these submounts are maintained under more realistic bonding conditions, namely at 320 °C for up to 20 s, pitting phenomena are hardly observed and the surface of the solder pad is much smoother.

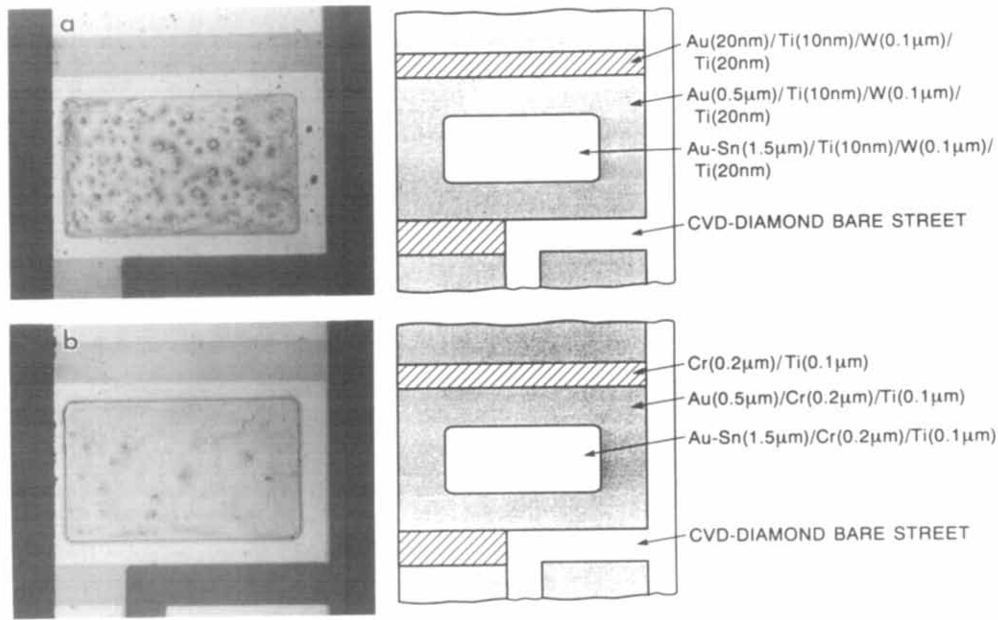

Fig. 21. Optical micrographs and schematic description of (a) W/Ti- and (b) Ti/Cr-based metallized CVD-diamond submounts after annealing at 320 °C for 1 min.

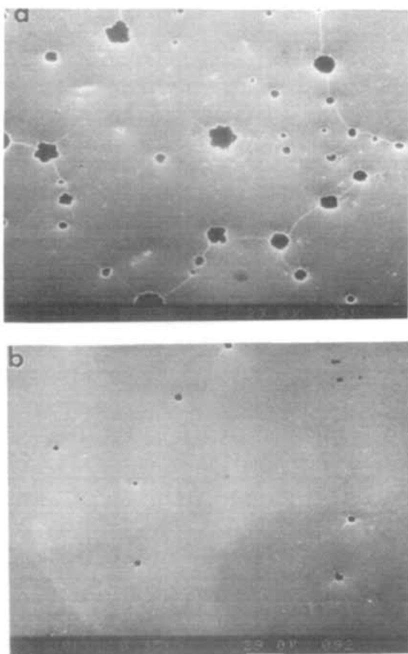

Fig. 22. SEM micrographs of (a) W/Ti/AuSn and (b) Ti/Cr/AuSn solder pads on CVD-diamond submounts after annealing at 320 °C for 1 min.

Figure 22 shows SEM micrographs of the Ti/W/Ti/AuSn (Fig. 22(a)) and Ti/Cr/AuSn (Fig. 22(b)) solder pad surfaces to demonstrate the density and size of the pits after reflow at 350 °C for 5 min. For the Ti/W/Ti system, the phenomenon appears to be more severe, with dense pitting and hole sizes of 2–20 μm. The small distance between the holes led to the formation of a crack network on the AuSn solder surface. For the Ti/Cr system the pit size is much more uniform ($\sim$2 μm) and the overall density of the pits is less than in the Ti/W/Ti system.

In order to define the interface in which the dewetting took place, an SEM/EDAX analysis was used and the results are shown in Fig. 23. For both the Ti/W/Ti/AuSn and Ti/Cr/AuSn systems, EDAX profiles were taken at a point on the solder surfaces (a_1 and b_1, respectively), and inside holes (a_2 and b_2, respectively). The EDAX spectrum of point a_1 shows only Au and Sn, while that of a_2 shows mainly W and a small amount of Ti. The spectrum of b_1 also shows only Au and Sn, while b_2 shows mainly Cr. From these data one can conclude that in both systems the formation of thermal stresses throughout the thermal cycle led to the 'ball up' and delamination of the AuSn solder from the Ti/W/Ti and Ti/Cr layers.

These phenomena can be disastrous when attempting to bond laser devices onto a submount, such as CVD-diamond. In Fig. 24 an example is given of a delamination of this type, which took place on a CVD-diamond submount subsequent to the bonding of an InP-based laser device onto it. The SEM micrographs clearly show the propagation of the delamination from mechanical damage that was introduced unintentionally into the solder pad during the bonding cycle. In this case, the mechanical delamination may lead to failure of the assembly as a result of the device losing adhesion and being sheared off the submount. Furthermore, and probably more disturbing, the delaminated metal flap may easily block the passage of light from the laser

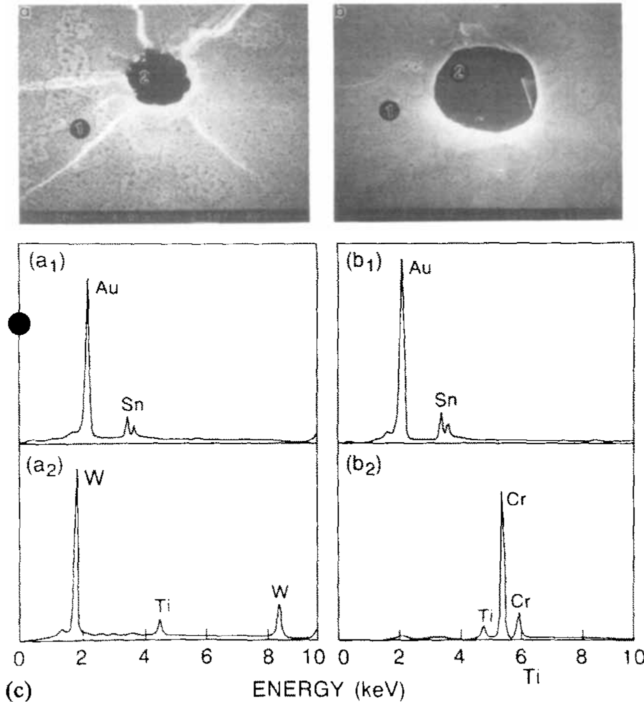

Fig. 23. SEM micrographs of the immediate area of a pit at the (a) W/Ti/AuSn, and (b) Ti/Cr/AuSn samples (Fig. 22), and EDAX analysis of the surface around the holes and inside the holes.

device, which is supposed to be incorporated into the attached fiber optics. This leads to optical failure of the entire packaged assembly, which is usually very costly.

In summary, both Cr and W metals provided excellent inert barrier metal layers under the AuSn solder when applying the Ti/Metal/AuSn scheme, which is the scheme typically used for bonding laser devices to CVD-diamond submounts. The eutectic composition and the liquid state of the solder were maintained at 320–350 °C throughout the entire bonding cycle and for a much longer thermal cycle (5 min) than were possible when bonding with Pt as the barrier layer (no longer than 15 s). This permits a major reduction in the AuSn solder pad thickness to about 0.5 μm, and thus improves the heat dissipation from high-power laser devices.

Ti/W_x $metal_y$/AuSn bonding schemes

Introduction

In the previous section, we discussed the major disadvantage of Ti/Cr/AuSn and Ti/W/Ti/AuSn, namely the poor wettability of the AuSn solder onto the barrier metals, as a result of the almost completely inert nature of both W and Cr to AuSn. In order to improve the wetting performance of the solder to the submount while maintaining the extremely long AuSn freezing time as a result of the inert interfacial nature, we extended our investigation of adhesion and wetting layers to be introduced between the barrier metal layer and the solder. This concept is illustrated schematically in Fig. 25, and its nature and performance are discussed below.

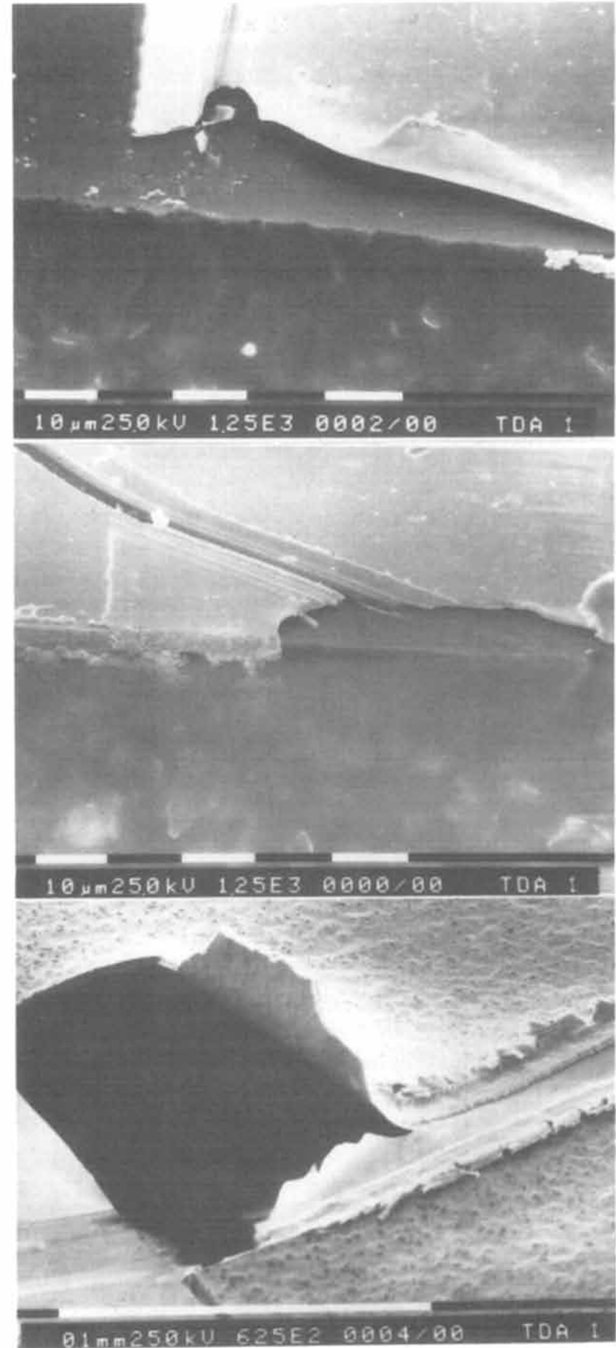

Fig. 24. SEM micrographs of examples of AuSn solder delaminated from metallized CVD-diamond submount.

Conceptual approach

Samples of Ti/W/AuSn, Ti/WAu/AuSn, Ti/W(AuSn)/AuSn and Ti/W(Ni_3Sn_2)/AuSn systems were studied; the actual structures are given in Table 1. A summary of the AuSn solder surface local freezing times (SLFT)

Fig. 25. Schematic presentation of conceptual design of advanced bonded device assembly.

and global freezing times (GFT), which were measured while heating the samples under forming gas at ambient and in liquid flux, is given in Table 2, and will be discussed in detail later. The quality of the adhesion between the solder and the metal layer structure is also given in this table, in order to provide a qualitative measure of the integrity of the metallization schemes. These results and the SEM–EDS, RBS and AES data will be discussed.

Ti/W/AuSn

The Ti(100 nm)/W(200 nm)/AuSn(3000 nm) system, which was studied as the basic metallization scheme used for bonding of the InP laser diode to the heatsink, was discussed earlier in this review. The SLFT and GFT of this sample (see Table 2) were longer than 500 and 4000 s, respectively, which were the best freezing durations measured in the entire study. The lack of interfacial reaction between AuSn and W eliminated the degradation of the eutectic solder composition, and thus the premature solder freezing. However, this metallization provided insufficient adhesion of the solidified solder to the metallization under it, as a result of poor wetting performance during the melting, while reflowing the solder.

Ti/W/WAu/Au/AuSn [30]

The Ti/W/WAuSn/AuSn system was proposed in order to improve the adhesion of the AuSn solder to the W barrier layer. The system studied comprised the following multilayer scheme: Ti(100 nm)/W(100 nm)/WAu(200 nm)/Au(100 nm)/AuSn(300 nm). SLFT and GFT were measured to be only about 20 s and 500 s, respectively.

A generic mechanism to describe this melting, interactions and freezing of the solder, containing five stages, was assumed. First the Sn of the solder diffuses into the WAu codeposited layer. Subsequently, it reacts with the Au to form AuSn intermetallics which causes local Sn depletion zones at the solder and, as a result, premature local freezing in the liquid solder. After the formation of the AuSn intermetallics in the WAu codeposited layer and in the interface of the molten solder and the solid WAu codeposited layer, the in-diffusion rate of the Sn into the WAu layer is reduced and thus the GFT is extended significantly. Therefore, even after a long reflow (>10 min) at 320 or 350 °C, the AuSn solder did not solidify completely prior to turning off the plate and cooling the samples.

Thus, it is clear that by adding the codeposited WAu layer between the W and the AuSn, the adhesion of the metals was improved, however, at the price of significantly shortening the SLFT and GFT.

In addition, it was found that while heating the Ti/W/WAu/AuSn samples to a higher temperature of 350 °C, in both liquid flux and under forming gas, a limited dewetting was still observed. Figure 26(a) shows an optical micrograph of the sample that was reflowed under forming gas at 350 °C for 5 min. Figure 26(b)

TABLE 1. Metallization schemes studied to optimize bonding

Layer	1	2	3	4	5	6	7	8
AuSn solder (F)	AuSn (80% Au) 3 μm	AuSn (77.5% Au) 3 μm	AuSn (80% Au) 3 μm	AuSn (77.5% Au) 3 μm	AuSn (80% Au) 3 μm	AuSn (77.5% Au) 3 μm	AuSn (77.5% Au) 3 μm	AuSn (77.5% Au) 3 μm
Wetting layer (E)					Ni_3Sn_2 (200 nm)	Ni_3Sn_4 (100 nm)	Ni_3Sn_4 (200 nm)	Ni_3Sn_4 (400 nm)
Second adhesion layer (D)						$W(Ni_3Sn_4)_2$ (100 nm)		
First adhesion layer (C)		(WAu_2) (200 nm)	$W(AuSn)_2$ (200 nm)	$W(Ni_3Sn_2)_2$ (200 nm)	$W(Ni_3Sn_2)_2$ (200 nm)	$W(Ni_3Sn_2)_2$ (100 nm)		
Barrier layer (B)	W (100 nm)	W (100 nm)	W (50 nm)	W (50 nm)	W (50 nm)	W (50 nm)	W (50 nm)	W (50 nm)
Adhesion layer (A)	Ti (100 nm)	Ti (100 nm)	Ti (100 nm)	Ti (100 nm)	Ti (100 nm)	Ti (100 nm)	Ti (100 nm)	Ti (100 nm)

TABLE 2. Thermal stability and wetting performance of the various metallization structures studied

No.	Metallization scheme	Freezing time				W/AuSn Adhesion[a]			
		SLFT (s)		GFT (s)		Forming gas		PEG flux	
		320 °C	350 °C	320 °C	350 °C	320 °C	350 °C	320 °C	350 °C
1	Ti(100 nm)/W(100 nm)/AuSn(3 μ)	>500	>500	>4000	>4000	–	–	–	–
2	Ti(100 nm)/W(100 nm)/WAu_2 (200 nm)/AuSn(3 μ)	20	30	>500	>500	+	–	–	–
3	Ti(100 nm)/W(50 nm)/$W(AuSn)_2$-(200 nm)/AuSn(3 μ)	25	20	>500	>500	+	–	+	–
4	Ti(100 nm)/W(50 nm)/$W(Ni_3Sn_2)_2$-(200 nm)/AuSn(3 μ)	15	15	>500	>500	–	–	–	–
5	Ti(100 nm)/W(50 nm)/$W(Ni_3Sn_2)_2$-(200 nm)/Ni_3Sn_2(200 nm)/AuSn(3 μ)	75	65	>500	>500	+	+	+	+
6	Ti(100 nm)/W(50 nm)/$W(Ni_3Sn_2)_2$-(200 nm)/$W(Ni_3Sn_4)$(100 nm)/ Ni_3Sn_4(100 nm)/AuSn(3 μ)	180	180	>2000	>500	+	+	+	+
7	Ti(100 nm)/W(50 nm)/Ni_3Sn_4(200 nm)/ AuSn(3 μ)	300	300	>500	>500	+	–	–	–
8	Ti(100 nm)/W(50 nm)/Ni_3Sn_4(400 nm)/ AuSn(3 μ)	15	15	>500	>500	+	+	–	–

[a](–) poor wetting between AuSn and metal; (+) excellent wetting between AuSn and metal.

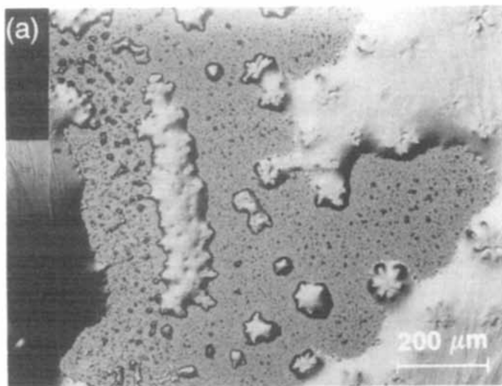

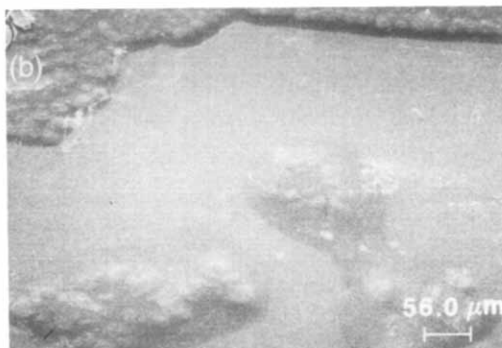

Fig. 26. SEM micrograph of Ti/W/WAu/AuSn sample, after reflow at 350 °C for 5 min, (a) under forming gas ambient and (b) in liquid flux–PEG400 bath.

shows the dewetting area of a similar sample that was reflowed at liquid flux.

As opposed to the EDS spectra that were collected on the dewetted area of the Ti/W/AuSn samples discussed earlier, the EDS spectrum of this sample exhibited detectable Au and Sn peaks, in addition to the observed Ti and W peaks. This result revealed that, in spite of the fact that dewetting occurred during the reflow, some degree of solder–barrier metal interaction indeed took place at the interface. In summary, it is clear that the addition of the AuW intermediate layer did improve the adhesion of the AuSn solder to the W barrier layer, by promoting interfacial mixing and interactions.

Ti/W/W(AuSn)/Au/AuSn

The Ti/W/WAuSn/Au/AuSn system was evaluated in order to further improve adhesion of the AuSn solder to the W barrier layer. The sample comprised the following layer structure: Ti(100 nm)/W(50 nm)/ $W(AuSn)_2$(200 nm)/Au(100 nm)/AuSn(3000 nm). A small amount of Au was added to the solder in order to compensate for the extra amount of Sn at the $W(AuSn)_2$ interfacial layer.

SLFT and GFT of 25 and >500 s, respectively, were measured in this sample after reflow. The composition of the as-deposited AuSn solder was 81 wt.% Au–19 wt.% Sn, and the composition of the reflowed AuSn

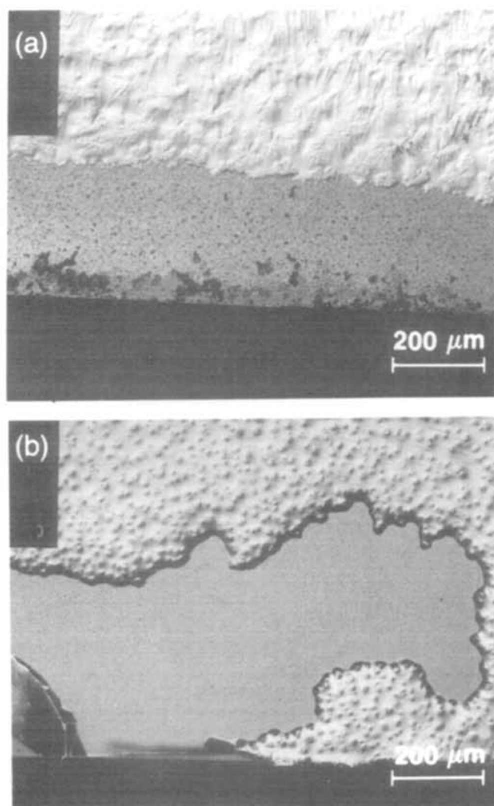

Fig. 27. Optical micrograph of Ti/W/W(AuSn)/AuSn sample after reflow at 350 °C for 5 min, (a) under forming gas ambient and (b) in liquid flux–PEG400 bath.

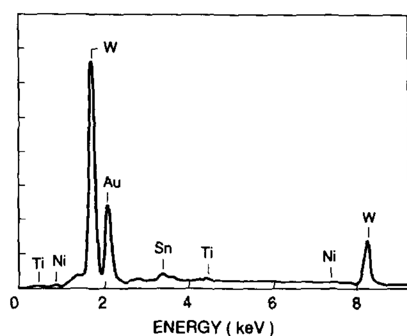

Fig. 28. EDS spectrum of a dewetted area at the Ti/W/W(AuSn)/AuSn sample, after reflow at 320 °C for 5 min in liquid flux–PEG400 bath.

solder was found to be 80 wt.% Au–20 wt.% Sn, which was almost the same as that of the as-deposited solder.

In this sample the solder did not ball up on heating to 320 °C, either at liquid flux or under forming gas. But solder balls were observed when the sample was heated to 350 °C. Figure 27 shows optical micrographs of the dewetted area of the forming gas-reflow sample (Fig. 27(a)) and of the flux–reflow sample (Fig. 27(b)).

EDS profiles were taken at dewetted areas, and an example is shown in Fig. 28. Au and Sn signals were also detected by the EDS in addition to Ti and W peaks. This suggested that some limited level of interaction between the metals and the solder took place also in this system prior to dewetting.

Ti/W/W(Ni_3Sn_2)$_2$/Au/AuSn

The Ti/W/W(Ni_3Sn_2)$_2$/Au/AuSn metallization scheme was the next system that was evaluated, introducing the W(Ni_3Sn_2)$_2$ codeposited film as a transition layer to improve the adhesion between the AuSn solder and the W barrier layer. The structure that was studied comprised six layers in the following order: Ti(100 nm)/W(50 nm)/W(Ni_3Sn_2)$_2$(200 nm)/Ni_3Sn_2(200 nm)/Au(100 nm)/AuSn(3000 nm). The motivation for introducing a NiSn intermetallic layer was to improve the adhesion of the AuSn to the inert underlying layer. This role of the NiSn compound, discussed earlier in the literature, suggests that the mechanism responsible for the adhesion improvement induced by these intermetallics is attributed to its performance as an excellent wetting layer due to the enhanced formation of the Sn-rich alloys, such as Ni_3Sn_2 and Ni_3Sn_4 [19–22]. As a result of these reactions the Sn at the AuSn solder layer depletes relatively rapidly and thus in order to compensate for this depletion, a Sn-rich AuSn solder (24 wt.% Sn) was applied into this system.

Figure 29 provides the AES profiles of the as-deposited Ti/W/W(Ni_3Sn_2)$_2$/Ni_3Sn_2/Au100/AuSn sample (Fig. 29(a)), and of the same sample after reflow at 350 °C for 5 min (Fig. 29(b)). It was observed that the initial solder layer (3 μm thick) having a Sn-rich solution of 76:24 (wt.%) Au:Sn, underwent a significant intermetallic reaction during the heating cycle, which resulted in an increase in thickness to about 3.9 μm and in a depletion of the Sn concentration at the solder to a final stoichiometry of Sn:Au 20:80 wt.%.

The presence of the NiSn layer was found to improve the integrity of the overall multilayer structure, as was reflected in the excellent adhesion of the AuSn solder to the W layer. The SLFT was measured to be longer than 50 s and GFT longer than 500 s.

Figure 30 shows a SEM micrograph of the Ti/W/W(Ni_3Sn_2)$_2$/Ni_3Sn_2/Au100/AuSn system after reflow at liquid flux at 350 °C for 5 min. The typical phase-separation morphology of a eutectic reaction is clearly observed. As anticipated from the evaluation of the AuSn phase diagram, pure AuSn compound and other Au and Sn solid intermetallics were present in the solidified structure. The brighter phase was identified by EDS as the Au_4Sn compound, as shown in Fig. 31(a), and the darker area was identified to be AuSn, as shown in Fig. 31(b). The excellent stability of this system during the reflow heating cycles, at temperatures as high as 350 °C for a duration of 5 min, is clearly shown as well at the AES depth profile (Fig. 29). One can observe the extent of the WNiSn interfacial reaction,

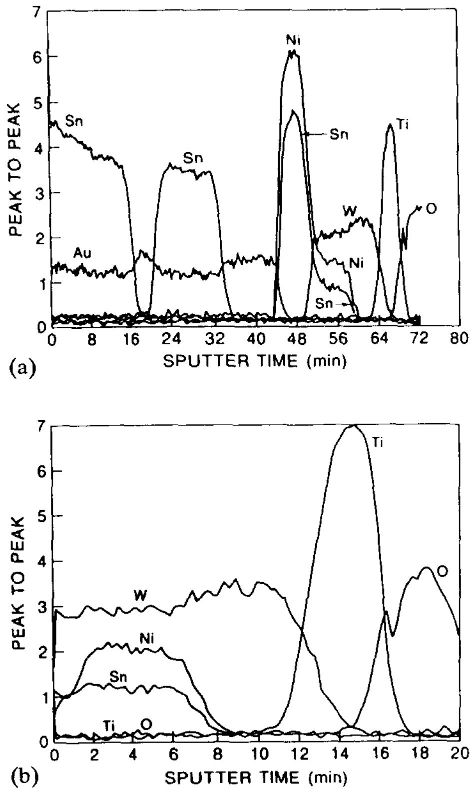

Fig. 29. AES depth profiles of the (a) as-deposited Ti/W/ $W(Ni_3Sn_2)_2/Ni_3Sn_2/Au/AuSn$ sample, and (b) this sample after reflow at 350 °C for 5 min.

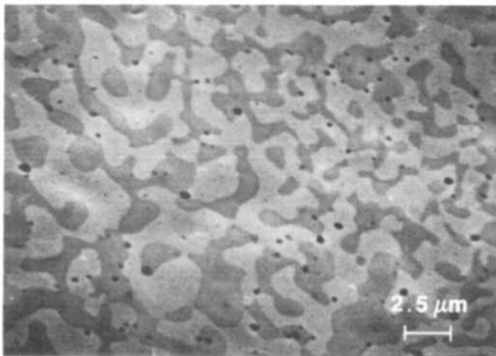

Fig. 30. SEM micrograph of AuSn eutectic structure formed on the $Ti/W/W(NiSn)/Ni_3Sn_2/AuSn$ sample after reflow at 300 °C for 5 min under forming gas ambient.

which took place in the system and enhances the adhesion of the AuSn to the W while leaving unreacted W under it to allow good barrier performance.

$Ti/W/W(Ni_3Sn_4)/Ni_3Sn_4/Au/AuSn$

Ti(100 nm)/W(50 nm)/$W(Ni_3Sn_4)$(100 nm)/Ni_3Sn_4-(100 nm)/Au(100 nm)/AuSn(3000 nm) system was the final modified system that was evaluated in an attempt to extend the SLFT of the previous systems. In this case, two codeposited layers with different codeposited ratios of W and Ni_3Sn_4 were introduced between the solder and the W barrier layer in order to provide a better chemical gradient in the transition from the pure W layer to the AuSn solder. A Sn-rich solder was also introduced onto this sample.

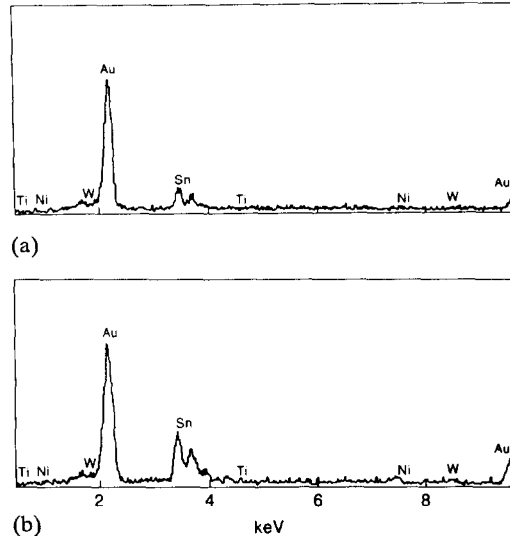

Fig. 31. EDS spectra of eutectic AuSn solder in the Ti/W/ W(NiSn)/NiSn/AuSn sample after reflow at 320 °C for 5 min under forming gas ambient; (a) at the white area of the eutectic solder, and (b) at the black area of the eutectic solder.

The motivation for adding the Ni_3Sn_4 intermetallic compound layer was to improve the adhesion of the AuSn solder to the underlying W layer, while minimizing the solder to barrier interfacial reaction. This is essential in order to eliminate the dilution of the Sn from the AuSn solder, which eventually leads to degradation of the eutectic composition and to premature freezing of the solder. The Ni_3Sn_4 is a promising candidate to fulfill this goal, since it is saturated with Sn and thus will not consume further Sn from the adjacent AuSn solder. Indeed, SLFT of longer than 200 s while heating at temperatures of 320–350 °C were measured for this sample, and a GFT longer than 60 min was measured.

In order to evaluate the quality of the solder wetting performance, and the nature of the molten solder flow, four different samples with various metallization pad sizes under the solder pad were prepared and tested. These metallization areas are designed to allow the flow of excess molten solder away from the joint-bonded volume under the device. Figure 32 provides optical micrographs of two of the above submounts after reflow under forming gas at 350 °C for 5 min. One can see that the molten solder has flowed to the edges of the metallization pad and completely covered it, regardless of the metallization area size. Even the largest metallization pad, which is shown on the right-hand micrograph of Fig. 33, has been completely covered with molten solder in a uniform fashion by the end of the reflow cycle. This suggests that excellent solder stability

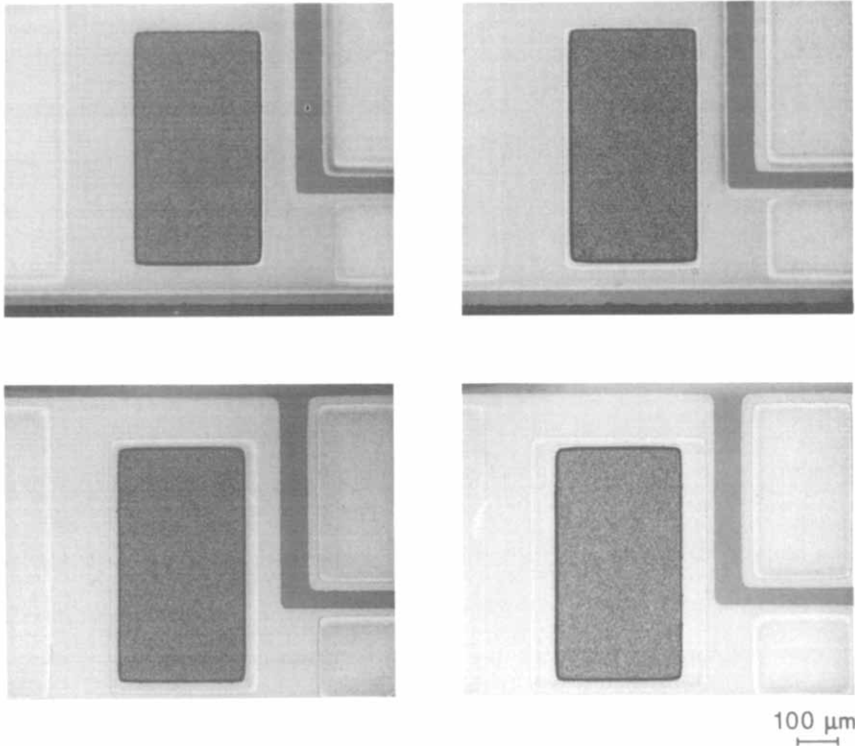

Fig. 32. Optical micrographs of four $Ti/W/W(Ni_3Sn_4)/Ni_3Sn_4/Au/AuSn$ metallized submounts, differing from each other by the dimension of the Au-capped solder flowing area under the solder pad.

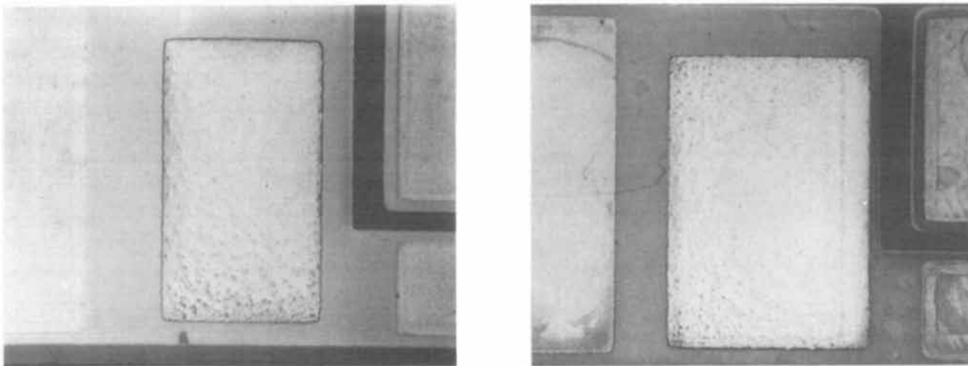

Fig. 33. Optical micrographs of two $Ti/W/W(Ni_3Sn_4)/Ni_3Sn_4/Au/AuSn$ metallized submounts, after reflow in liquid flux at 350 °C for 5 min.

was achieved and, as observed previously, the 80:20 Au:Sn eutectic composition was maintained even during the very long (> 60 min) reflow process, with an excellent solder-to-barrier wetting performance. Figure 34 provides optical micrograph of the solder after undergoing a reflow cycle at 320 °C for 5 min. One can observe the uniform and integrated appearance of the metallization, which has a typical eutectic phase-separation morphology, indicating that the composition of the resolidified solder remained close to the eutectic composition. As predicted from the phase diagram, the Au_4Sn and AuSn solid intermetallics were, indeed, formed and observed in the frozen AuSn eutectic structure.

Figure 35 provides the AES spectra of the $Ti/W/W(Ni_3Sn_4)/Ni_3Sn_4/Au/AuSn$ as deposited and after reflow at 320 °C and 350 °C for 5 min. It is clear that the presence of the $W(Ni_3Sn_4)$ wetting layer significantly improved the integrity of the overall multilayer structure resulting in perfect adhesion of the AuSn solder to the W layer. Thus, the application of a W layer as a reaction barrier under the AuSn solder, in which reaction of the AuSn solder with the barrier metals is essentially eliminated, is seen to provide a superior bonding system.

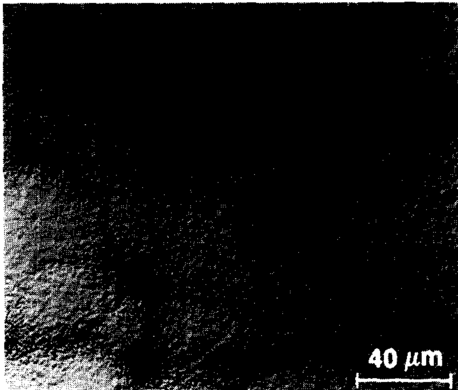

Fig. 34. Optical micrograph of the AuSn eutectic structure formed on the Ti/W/W(Ni_3Sn_4)/Ni_3Sn_4/AuSn sample, after reflow at 350 °C for 5 min under forming gas ambient.

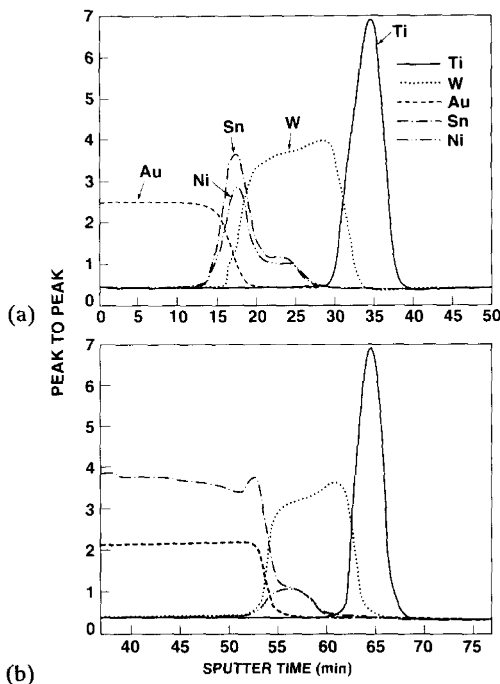

Fig. 35. AES profiles of the Ti/W/W(Ni_3Sn_4)/Ni_3Sn_4/Au/AuSn samples, (a) as-deposited, and (b) after reflow under forming gas at 320 °C for 5 min.

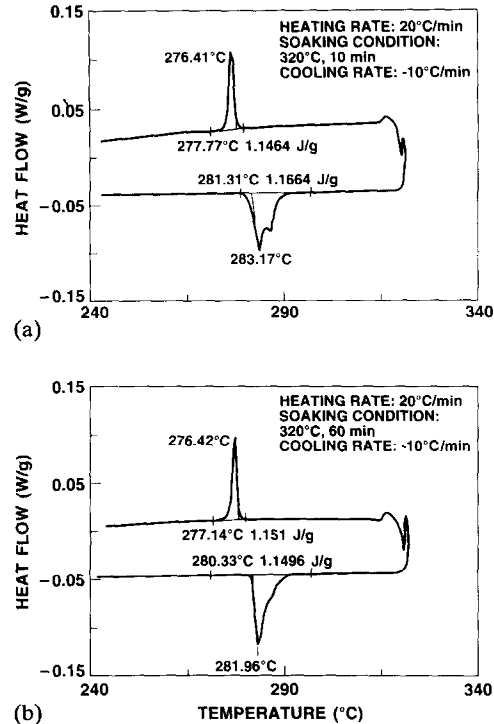

Fig. 36. DSC spectra of Ti/W/W(Ni_3Sn_4)/Ni_3Sn_4/Au/AuSn sample that was heat-treated at 320 °C (a) for 10 min, and (b) for 10 min, cooled to 200 °C, and heated again to 320 °C for 60 min under N_2 gas ambient.

Figure 36(a) shows the DSC results (without scan rate calibration) of the Ti/W/W(Ni_3Sn_4)/Ni_3Sn_4/AuSn sample, which was heat-treated at 320 °C for 10 min. The heat of melting (based on total weight of the system) is shown to be about 0.8165 J g^{-1}. The solder started to melt at 281.3 °C. After annealing at 320 °C for 10 min, on cooling the solder solidified at 277.8 °C with a heat release of 0.8025 J g^{-1}. The difference between the heats of absorption and evolution of this metallization–thin solder system after heat treatment at 320 °C for 10 min is less than 2%, which is within experimental scatter. This is in contrast to the previous DSC study of Ti/Pt/AuSn system, in which the sample, when heated at 320 °C for 10 min, solidified completely and showed no indication of freezing upon cooling through the eutectic melting temperature of AuSn. Such behavior indicates that this metallization–thin solder system is so stable that the total amount of the compounds which comprises the eutectic solder in the system has changed only slightly during the heat treatment.

In order to evaluate the reproducibility of the melting, the sample which had been annealed at 320 °C for 10 min was reheated to 320 °C and held at this temperature for 60 min. Figure 36(b) gives the DSC results of this experiment. The heat of melting was measured this time to be 0.8017 J g^{-1} and the melting temperature 280.3 °C. After heat treatment at 320 °C for 60 min, the sample heat of solidification was measured to be 0.8057 J g^{-1} and the freezing temperature 277.1 °C. The heat of melting and solidification measured in the previous run and in this run were nearly identical. This provides a strong evidence to the fact that the solder has not been prematurely frozen even after many thermal cycles have been executed.

Figure 37(a) provides the DSC results of a sample that was heat-treated at 350 °C for 10 min. The heat of melting was found to be 0.8028 J g^{-1} and the melting temperature 281.3 °C. After heat treatment, the heat of solidification was measured to be 0.7909 J g^{-1} and

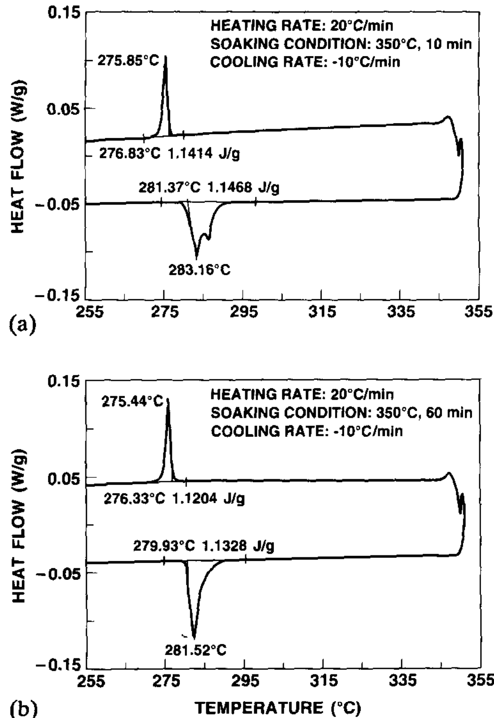

Fig. 37. DSC spectra of Ti/W/W(Ni_3Sn_4)/Ni_3Sn_4/Au/AuSn sample that was heated to 350 °C (a) for 10 min, and (b) for 10 min, cooled to 200 °C and heated again to 320 °C for 60 min under N_2 gas ambient.

the freezing temperature 276.8 °C. The heats evolved through melting and solidification are very similar, suggesting again the high stability of this system.

Multicycle reflows of this sample were conducted at 350 °C as well. Figure 37(b) shows the DSC results of the second thermal cycle of the testing. The heat of melting was found to be 0.7930 J g^{-1} and the melting temperature 279.9 °C. After a further heat treatment at 350 °C for 60 min, the heat of solidification was measured to be 0.7843 J g^{-1} and the solidification temperature 275.4 °C. The heats of melting and solidification measured in the first run and the second run were nearly identical. The fact that the solidification temperature was so well conserved provides strong evidence that the solder composition has not changed through these very severe thermal cycles.

In summary, it appears that the five layered Ti/W/W(Ni_3Sn_4)/Ni_3Sn_4/Au/AuSn system provides the best bonding metallization scheme of all the systems that were evaluated through the current study.

Conclusions

In this review we attempted to examine the performance of the most commonly used metallurgical schemes for the bonding of high-power laser devices onto submounts, and in particular onto CVD-diamond submounts.

In the standard configuration, a 3 μm layer of eutectic AuSn (80 wt.% Au) solder (T_m=278 °C) is deposited onto a 0.2 μm Pt barrier layer, which caps a 0.1 μm Ti adhesion layer adjacent to the submount. This system is easy to deposit and permits good bonding of the device to the submount. The Ti/Pt/AuSn system, and particularly the Pt/AuSn interface, is very reactive thermodynamically, mainly as a result of the almost spontaneous reactions that take place between Pt and Sn, even at room temperature. As a result the Pt consumes Sn from the AuSn to form interfacial PtSn intermetallics through solid state reactions, diluting the Sn from the solder and thus deteriorating the eutectic stoichiometry composition. The stoichiometry varies even further once the solder melts during the bonding cycle, dissolving more Pt into the solder, and leading to premature solidification of the solder. Thus special precautions must be taken during deposition of the various layers and during the bonding process, to limit heating of the multilayer structure and thus limit metallic interactions. It is clear that the Ti/Pt/AuSn bonding metallization scheme is not a robust one, and provides a very narrow processing window (for both temperature and time) to complete a successful bonding cycle.

In order to improve the bonding process, a more stable metallurgical system is needed. This may involve either replacement of the AuSn solder by a less reactive one, or the use of an alternative barrier layer metal, or both. For InP-based laser bonding applications, it is, unfortunately, impossible to introduce a more stable solder, which by definition will have higher melting and bonding points, since the laser device undergoes accelerated degradation at temperatures higher than 320 °C. Therefore the more attractive solution is to evaluate an alternative and advanced barrier metallization schemes under the AuSn solder, in order to stabilize the metallurgical scheme and allow for a superior and more robust bonding assembly. The quality of the advanced bonding metallization schemes was evaluated through the thermodynamic stability of the solder, once melted. This was reflected by both the surface and the global freezing times of the solder, as well as the adhesion of the molten and solidified AuSn solder to the various barrier metals. A minimum interaction between the AuSn solder and the barrier metals is required to eliminate solder deterioration, and thus allow for a long solder nonfreezing period. The applied metallization should, however, undergo some interaction with the solder in order to promote sufficient adhesion of the barrier metals to the solder. The microstructure of the various metallization systems, as deposited and

after reflow at both N_2 ambient and in liquid flux, were studied in detail, and the correlation between it and the solder refreezing time was evaluated.

The first set of systems tested contained a conceptually similar structure, of 0.1 μm Ti as an adhesion layer adjacent to the submount, capped with 0.2 μm of barrier metal, onto which 3 μm of AuSn solder was deposited. Ni, Cr and W were evaluated as potentially superior barrier layer metals. All of the above metals were found to be less reactive with the AuSn than was Pt; W was found to be absolutely inert. Surface local freezing and global freezing phenomena were not observed during reflow in forming gas or flux, but the solder had dewetted from the W layer, reflecting insufficient interaction and adhesion of the solder to the W layer.

Therefore, it was concluded that in order to maintain good stability of the solder on the barrier metal, as observed in the Ti/Pt/AuSn system, but improve the adhesion of the solder, the simple bonding metallization schemes were not sufficient, and more complicated systems had to be applied. Not only are adhesion and barrier metal layers required at the submount and under the solder, but an additional adhesion layer must be added between the barrier and the solder layers, to improve the integrity of the entire system.

The first multilayer that was studied was the Ti/W/WAu/AuSn system. The adhesion of the solder was improved somewhat, by introducing a WAu codeposited layer between the solder and the W layer. By reflowing the sample under forming gas at 320 °C, good integrity of the solder to W layer was achieved; however, dewetting still took place at the higher reflow temperature of 350 °C. Reflowing the sample at liquid flux resulted in complete delamination of the solder from the W layer, even at the lower temperature of 320 °C.

Further improvement in system integrity was obtained by using the Ti/W/W(AuSn)/AuSn system. Introducing an improved ternary wetting layer between the AuSn solder and the W layer resulted in entirely eliminating delamination of the solder from the W layer during reflowing of the sample at 320 °C. Occasional dewetting of the solder from the W layer was, however, still observed during heating the sample at higher temperatures. The improved stability led to extension of the solder local freezing time to about 25 s, and more than 500 s were required for complete solidification of the solder.

Final modification and optimization of the bonding scheme were achieved by adding a second wetter layer between the adhesion layer and the solder. The entire metallurgical scheme became a 5-layer structure, with the following composition: Ti/W/W(Ni_3Sn_4)/Ni_3Sn_4/AuSn. This system showed excellent thermal stability at all treatment temperatures. Surface local freezing time was measured to be longer than 200 s and the global freezing time was found to be longer than 60 min. No dewetting whatsoever was observed in the reflow samples, regardless of the ambient. Thus, it was concluded that introduction of two adhesion layers between the AuSn solder and the W barrier layer provided the optimum solution for achieving perfect adhesion and integrity of the entire multilayer structure, without sacrificing the excellent inert nature of the AuSn solder to the barrier metal provided by the presence of the W layer.

Thus, it is seen that in order to achieve a robust bonding metallization system, a sophisticated and advanced multilayer technology must be applied. This provides a great challenge to materials and process engineers and designers. The same skills and talent that traditionally were invested in developing stable and robust metal contacts to the semiconductor devices must be used to develop modern bonding metallization schemes as well. Multilayer structures are essential in order to achieve the required device-to-submount bonded assembly integrity. Furthermore, by developing solutions to both the device contacts and submount bonding metallization schemes, which each have special tasks and goals, the metallurgical engineer has to be concerned about the compatibility of both complicated metallizations.

Acknowledgements

The collaboration and hard work of H.S. Chen, D.D. Bacon, F. Baiocchi, E. Lane and C. Doherty, in realizing and carrying out this study, are greatly appreciated.

References

1 K. Das, V. Venkatesan, K. Miyata, D.L. Dreifus and J.T. Glass, in Y. Tzeng, M. Yoshikawa, M. Murakawa and A. Feldman (eds.), *Applications of Diamond Films and Related Materials*, Elsevier, Amsterdam, 1991, pp. 301–308.
2 A.T. Collins, *Semicond. Sci. Technol., 4* (1989) 605.
3 J.E. Graebner, S. Jin, J.A. Herb and C.F. Gardinier, *Appl. Phys. Lett., 60* (1992) 1576.
4 J.E. Graebner, S. Jin, G.W. Kammlott, J.A. Herb and C.F. Gardinier, *Nature, 359* (1992) 401.
5 *Wall Street Journal*, October 13 (1992)
6 *Diamond and Structural Carbon News*, October (1992).
7 C.C. Lee, C.Y. Wang and G.S. Matijasevic, *IEEE Trans. Comp. Hybrids, Manuf. Technol., 14* (1991) 407.
8 J.H. Lau and D.W. Rice, *Solid-State Technol., 28* (1985) 91.
9 S. Knecht and L.R. Fox, *IEEE Trans. Comp. Hybrids, Manuf. Technol., Chmt-9* (1986) 423.
10 O. Wada and T. Kumai, *Jpn. J. Appl. Phys., 40* (1991) L1056.
11 G.S. Matijasevic and C.C. Lee, *Proc. IEEE Int. Reliability Physics Symp.*, Phoenix, AZ, November, 1989.
12 O. Wada and O. Ueda, in A. Katz, S.P. Muraka and A. Appelbaum (eds.), *Advanced Metallization in Microelectronics*, Mat. Res. Soc. Symp. Proc. 181, MRS, Pittsburgh, 1990, pp. 273–280.

13 W.G. Bader, *Welding Res. Suppl., 48* (1969) 551.
14 O. Wada and T. Kumai, *Appl. Phys. Lett., 58* (1991) 908.
15 C.Y. Wang and C.C. Lee, *IEEE Trans. Comp. Hybrids, Manuf. Technol., 14* (1991) 874.
16 H. Okamota and T.B. Massalski, in T.B. Massalski (ed.), *Binary Alloy Phase Diagrams,* AMS, Ohio, 1991, p. 403.
17 P.J. Kay and C.A. Mackay, *Trans. Inst. Met. Finish., 54* (1976) 68.
18 R.J. Klein Wassink in *Soldering in Electronics,* Electrochemical Publications, Ayr, UK, 1989, p. 179.
19 P. Nash and A. Nash, in T.B. Massalski (ed.), *Binary Alloy Phase Diagrams,* AMS, Ohio, 1991, p. 2864.
20 W.J. Tomlinson and H.G. Rhodes, *J. Mater. Sci., 22* (1987) 1769.
21 A.C. Harman, *Proc. Technical Programme Internepcon 1978,* Brighton, UK, pp. 42–49.
22 P.J. Kay and C.A. Mackay, *Trans. Inst. Met. Finish., 57* (1979) 169.
23 N.G. Koopman, T.C. Reiley and P.A. Totta, in R.R. Tummala and E.J. Rymaszewski (eds.), *Microelectronics Packaging Handbook,* Van Nostrand Reinhold, New York, 1989, p. 395.
24 K. Mizuishi and T. Mori, *IEEE Trans. Component Hybrids Manuf. Technol., Chmt-11* (1988) 481.
25 A. Katz, F. Baiocchi, E. Lane, C.H. Lee, C. Hall, J. Doting, C. Gritsbach and K. Harris, *J. Appl. Phys.,* to be published.
26 *US Pat. 005 197 654* (1993) to A. Katz, C.-H. Lee, K.L. Tai and Y.-M. Wang.
27 A. Katz, K.-W. Wang, F.A. Baiocchi, W.C. Dautremont-Smith, E. Lane, H.S. Luftman, R.R. Varma and H. Curnan, *J. Appl. Phys., 72* (1992) 3808.
28 R. Darshmukh, E. Laskowski and J. Shmulovich, private communication.
29 S. Nakahara, R.J. McCoy, L. Buene and J. Vanderberg, *Thin Solid Films, 84* (1981) 185.
30 *US Pat. 5 234 153* (1993), to A. Katz, D.D. Bacom, C.-H. Lee, K.L. Tai and Y.-M. Wang.